Fluid Models for Kinetic Effects on Coherent Nonlinear Alfvén Waves. II. Numerical Solutions

M. V. Medvedev[1, *, †], V. I. Shevchenko[2], P. H. Diamond[1, ‡], and V. L. Galinsky[3]

[1] *Physics Department, University of California at San Diego, La Jolla, California 92093-0319*
[2] *Electrical & Computer Engineering Department, University of California at San Diego, La Jolla, California 92093-0407*
[3] *Scripps Institution of Oceanography, University of California at San Diego, La Jolla, California 92093-0210*

The influence of various kinetic effects (e.g. Landau damping, diffusive and collisional dissipation, and finite Larmor radius terms) on the nonlinear evolution of finite amplitude Alfvénic wave trains in a finite-β environment is systematically investigated using a novel, kinetic nonlinear Schrödinger (KNLS) equation. The dynamics of Alfvén waves is sensitive to the sense of polarization as well as the angle of propagation with respect to the ambient magnetic field. Numerical solution for the case with Landau damping reveals the formation of dissipative structures, which are quasi-stationary, S-polarized directional (and rotational) discontinuities which self-organize from parallel propagating, linearly polarized waves. Parallel propagating circularly polarized packets evolve to a few circularly polarized Alfvén harmonics on large scales. Stationary arc-polarized rotational discontinuities form from obliquely propagating waves. Collisional dissipation, even if weak, introduces enhanced wave damping when β is very close to unity. Cyclotron motion effects on resonant particle interactions introduce cyclotron resonance into the nonlinear Alfvén wave dynamics.
PACS numbers: 96.50.Ci, 52.35.Mw, 52.35.-g, 95.30.Qd

I. INTRODUCTION

The envelope dynamics of nonlinear Alfvén waves at small-β are thought to be governed by the derivative nonlinear Schrödinger (DNLS) equation, which describes parametric coupling with acoustic modes [1]. It is believed that the dynamics of such waves changes drastically in a collisionless, finite-β plasma, due to several kinetic effects, especially collisionless (Landau) damping of ion-acoustic oscillations [2–4]. In a highly dissipative regime, the ion-acoustic *quasi*-mode is no longer a plasma eigenmode. Thus, it is more natural (according Refs. [5,6]) to view the mechanism of Landau damping of Alfvén waves as particle trapping by both the magnetic mirror force and electric field. On account of the inevitable mathematical difficulties of a kinetic approach, many numerical simulations have been performed. DNLS-based simulations with beam pumping (comet modeling) [7,8], hybrid magnetohydrodynamic-particle simulations [9,10], hybrid particle ions-fluid electrons simulations [11–13] have been performed.

In a previous paper [14], we systematically accounted for ion kinetic effects (but neglected finite conductivity, discussed elsewhere [3,15]) on parallel and slightly oblique propagating waves in homogeneous plasma, to the order at which the DNLS is derived. A fluid representation for Landau damping [16] allowed us to derive a relatively simple evolution equation for finite amplitude Alfvén waves in finite-β environments, typical of the solar wind. Collisional damping was also included. For slightly oblique propagation, the effects of finite Larmor radius result in nonlinear dispersion-type integral terms. The terms which describe kinetic effects are usually integral (nonlocal) in nature, and reflect the finite ion transit time through the envelope modulation of an Alfvén train. However, for the weakly collisional (viscous) dissipation and for the small Larmor radius limits, these integral operators asymptote to (local) differential operators. This is not the case for Landau damping, since no intrinsic scale exists. The envelope evolution equation obtained is thus a nonlocal, integro-differential equation which is not not amenable to *analytical* solution.

In this paper, we explore numerical solution of the kinetically modified derivative nonlinear Schrödinger (KNLS) equation. Some preliminary results of this investigation are given in Ref. [17]. We again classify the solutions by the kinetic effects which are taken into count. For simplicity, we usually consider parallel propagating waves, however the results are valid for oblique waves since they still obey the KNLS equation [18,19,14].

We discover that (especially for the case of Landau damping) new types of waveform emerge. The known observed "final states" of nonlinear wave steepening (i.e. shock structures) are classified as:

1.) *collisional* (hydrodynamic) *shocks* for which nonlinear steepening is limited by *collisional* (viscous) dissipation, which sinks energy from small scales (i.e. from high-k harmonics);

2.) *collisionless shocks* (common in astrophysical plasma) in which nonlinear steepening is limited by *dispersion* resulting in soliton-type structures with sufficient energy content in high-k harmonics.

*E-mail: mmedvedev@ucsd.edu Internet: http://sdphpd.ucsd.edu/~misha/mm.html
†Also at the Institute for Nuclear Fusion, Russian Research Center "Kurchatov Institute", Moscow 123182, Russia.
‡Also at General Atomics, San Diego, California 92122.

A new, large class of waveforms, *dissipative structures*, appears when dissipation acts on all scales (recall Landau damping has no intrinsic characteristic scale). Thus, we add

   3.) *dissipative structures*, for which nonlinear steepening is limited by *collisionless* (scale invariant) damping. Harmonic spectra of such structures contain predominantly low-k harmonics, i.e. energy resides at small scales. Fast rotation of the of wave magnetic field vector (i.e. rotational or directional discontinuity formation) is another common feature of these structures.

Dissipative structures emerge in plasma with $T_i \sim T_e$ for a wide range of β: $0.5 \le \beta \le 1.5$, which is typical for the solar wind plasma. Thus, we argue that such structures are likely a common constituent of solar wind Alfvénic turbulence. Note here that the dissipative structures discussed here emerge without external energy source in the system. Thus, the amplitude of them decreases with time.

Numerous *in situ* observations of the solar wind magnetic activity have revealed the nonlinear nature of MHD waves [20,21]. Recent observations indicate the existence of directional (e.g. rotational) discontinuities, i.e. regions of rapid phase jumps where the amplitude also varies [20,22]. Several types of directional/rotational discontinuities which might be distinguished by their phase portraits have been observed. There are (i) discontinuities of the "S-type", at which the magnetic field vector rotates first through some angle (less than or close to $90°$) in one direction, followed by rotation in the opposite direction through an angle larger than $180°$ (typically, $180° < \Delta\phi \le 270°$) [22,23], and (ii) arc-polarized discontinuities, where the magnetic field vector rotates along an arc through an angle less than $180°$ [20,24]. At directional discontinuities, the fast phase jump is accompanied by moderate amplitude modulation ($\delta B \sim B$). At the rotational discontinuities, the amplitude modulation is small or negligible ($\delta B \ll B$). It is shown in this paper that all these commonly occurring wave structures are manifested in the nonlinear evolution of Alfvén waves in finite β, isothermal plasma for different initial conditions and propagation angle.

The theory of nondissipative Alfvén waves governed by the conservative DNLS equation predicts nonlinear wave steepening and formation of waveforms with steep fronts. These waveforms are unstable to modulations. Thus, spiky, many-soliton structures are emitted from the steep edge. These oscillatory, (roughly) circularly polarized soliton-like structes interact nonlinearly to yield strongly turbulent, spatially irregular wave profiles [see next section]. However, the DNLS theory fails to explain the formation of rotational and directional discontinuities. A further step was to include the linear damping of Alfvén waves due to finite plasma conductivity. It was shown that the nonlinear wave relaxes to a shock train and constant-B rotational discontinuities that rotate the

field through exactly $180°$ [25,26,1]. Inspite of this, the DNLS theory was unable to explain the existance and dynamics of both (i) the S-polarized directional and rotational discontinuities and (ii) arc-polarized rotational discontinuities with rotation of less than $180°$. Recent particle code simulations [11–13] have shown that Landau damping may drastically change the dynamics of Alfvén waves and result in the emergence of such wave structures.

In this paper, we use a recently developed [14] analytical model of the KNLS equation to investigate the influence of Landau damping and several other kinetic effects on the dynamics of Alfvén waves. The main claim of this paper is that *all* the discontinuous wave structures discussed above are *distinct solutions* of the same *simple* analytical model for different initial conditions, e.g. initial wave polarization and wave propagation angle. A (quasi-) parallel, initially circularly polarized, amplitude modulated wave evolves to a single, purely circular, lowest-k harmonic decoupled from dissipation. A (quasi-) parallel linearly polarized wave forms a *dissipative structure* which is characterized by S-type, fast phase rotation and moderate amplitude variation, i.e. has the requisite properties for classification as a localized, S-type directional/rotational discontinuity. Such discontinuities are intrinsically *dissipative*, as their amplitude continuously decreases with time. An obliquely propagating wave forms an arc-type rotational discontinuity, which does not experience even minimal dissipation. The effects of finite Larmor radius (significant at oblique angles) are shown to tend to suppress arc-polarized structure formation. Low-k, finite-amplitude circular waves form instead. Collisional (diffusive) dissipation of a ponderomotively driven acoustic mode is significant (even in a weakly collisional plasma) if the β value is close to unity, thus increasing plasma temperature in this region.

The remainder of this paper is organized as follows. In Section II, we discuss the method of calculation, initial conditions and standard DNLS solutions (i.e. the limiting case of $\beta = 0$). In Section III, we solve the KNLS for the case of Landau damping. In Section IV, we investigate an effect of collisional damping. In Section V, the influence of finite Larmor radius corrections on the dynamics of slightly obliquely propagating waves is investigated. Section VI presents a summary of the result obtained and some concluding remarks.

II. NUMERICAL METHOD, INITIAL CONDITIONS, AND DNLS SOLUTIONS

The general KNLS equation may be written as

$$\frac{\partial b}{\partial t_e} + \frac{1}{2}\frac{\partial}{\partial z}\left(U_{NL}b\right) + i\frac{v_A^2}{2\Omega_i}\frac{\partial^2 b}{\partial z^2} = 0, \qquad (1)$$

where $b = b(z - v_A t, t_e) = (b_x + ib_y)/B_0$ is the wave magnetic field, v_A and Ω_i are the Alfvén speed and proton ion-cyclotron frequency, and $t_e = (b^2/B_0^2)t$ represents

slow envelope evolution. The nonlinear ponderomotive plasma velocity perturbation is

$$U_{NL} = \frac{v_A}{2}\left(c_1\left(|b|^2 - \langle|b|^2\rangle\right) + c_2\widehat{\mathcal{K}}\left[|b|^2 - \langle|b|^2\rangle\right]\right). \quad (2)$$

Here c_1 and c_2 are functions of plasma parameters, i.e. β, T_e/T_i, etc., only. Throughout the paper, we set $T_e = T_i$ for simplicity. $\widehat{\mathcal{K}}$ is an integral operator which represents kinetic effects. The detailed form of it depends on the effects under consideration. We now introduce the dimensionless coordinate and time respectively as $\zeta = z/\bar{z}$ and $\tau = t_e/\bar{t}$, where $\bar{z} = 50c/\omega_p$ and $\bar{t} = 200/\Omega_i$. Here ω_p is the proton plasma frequency and c is the speed of light. Then, writing $b(\zeta,\tau) = L^{-1/2}\sum_k b_k \exp(i\lambda_k\zeta)$, where $\lambda_k = 2\pi k/L$ (L is the dimensionless domain length), the equation for k-th harmonic, b_k, follows as

$$\frac{\partial b_k}{\partial\tau} + i\eta\lambda_k^2 b_k \quad (3)$$
$$+ i\lambda_k\left\{c_1\left(|b|^2 - \langle|b|^2\rangle\right)b + c_2\widehat{\mathcal{K}}\left[|b|^2 - \langle|b|^2\rangle\right]b\right\}_k = 0,$$

where $\eta = 0.04$ is the dispersion parameter. This equation was solved for periodic boundary conditions using a predictor-corrector scheme and a fast Fourier transform to calculate nonlinearities.

For $\beta = 0$ no kinetics impacts the wave dynamics [14], so Eq. (1) reduces to the familiar DNLS equation with U_{NL} simply

$$U_{NL} = \frac{1}{2}\frac{v_A}{1-\beta}\left(|b|^2 - \langle|b|^2\rangle\right). \quad (4)$$

The DNLS is integrable and has the exact (soliton) solution [27–29,15]. We pick a standing (in the wave frame) soliton solution (b_0 is the soliton amplitude):

$$b(\zeta) = \frac{b_0\exp(i\Theta)}{\cosh\left[(\zeta - L/2)\,b_0^2/2\eta\right]}, \quad (5a)$$

$$\Theta(\zeta) = \frac{2}{3}\arctan\left\{\sinh\left[(\zeta - L/2)\,b_0^2/2\eta\right]\right\}. \quad (5b)$$

To avoid effects of periodic boundary conditions, we have chosen the domain length L equal to 32π and taken 8192 harmonics (and spatial points) so that $-4096 \le n \le 4096$. The test run has shown excellent agreement with the analytical solution during the time of computation (up to $\tau = 40$, i.e. 8,000 cyclotron periods).

As high-amplitude magnetic perturbations in the solar wind probably evolve from small-amplitude (linear) ones, it is reasonable to examine the nonlinear evolution of finite-amplitude periodic waves of both linear and circular polarizations. In these cases, we have taken $L = 4\pi$ and 1024 harmonics and spatial points, i.e. $-512 \le n \le 512$. Results of reference runs for amplitude modulated linear and circular polarizations are shown in Figs. 1 and 2, respectively. [Note here that only amplitude modulated waves experience nonlinear evolution, a purely circularly polarized wave with $b \sim \exp(i\lambda\zeta)$ is an

exact solution of the DNLS (and KNLS) for which nonlinear effects do not enter since $|b|^2 = 1$.] The initial wave profiles are given by two initially excited Fourier harmonics. For linear polarizations, we pick $b_{-1} = b_1 = 1$, all others are zeroes, for circular polarizations we pick $b_{-2} = b_{-1} = 1$, for elliptical polarizations, we pick $b_{-1} = 1.1$, $b_1 = 0.9$. Thus, the waves are left-hand polarized. However amplitude profiles, $|b|$ vs. ζ, (Figs. 1a, 2a) look alike, their phase portraits (Figs. 1b, 2b) and harmonic spectra (Figs. 1e, 2e) differ significantly. All the waves exhibit the nonlinear steepening phase of a front at earlier times ($\tau \sim 2$). Dispersion further limits steepening and produces (at times $\tau \sim 5$) small-scale parasitic, oscillatory, circularly polarized (even for initial linear polarization) wave structures. These oscillations are just DNLS solitons radiated from the steep front of the wave train by modulation instability. (By different authors, such a process is referred to as "dispersive steepening".) The direction of polarization is shown by an arrow on graphs 1b, 2b, indicating right hand polarization. At later times, $\tau \sim 40$, nonlinear processes result in a wave magnetic field which is completely irregular, as seen from Figs. 1c, 1d, 2c, 2d, as well as from their harmonic spectra, (Figs. 1e, 2e). In these cases strong, large-amplitude Alfvénic turbulence is developed.

III. COLLISIONLESS DISSIPATIVE ALFVÉN TRAINS

A. Numerical solutions

The KNLS equation with collisionless (Landau) dissipation [2–4,14,28,31] is Eq. (1), together with the nonlinear velocity perturbation written as

$$U_{NL} = \frac{v_A}{2}\left\{M_1\left(|b|^2 - \langle|b|^2\rangle\right) + M_2\widehat{\mathcal{L}}\left[|b|^2 - \langle|b|^2\rangle\right]\right\}, \quad (6)$$

where

$$M_1 = \frac{(1-\beta) + \widehat{\chi}_\parallel^2(1-\beta/\gamma)}{(1-\beta)^2 + \widehat{\chi}_\parallel^2(1-\beta/\gamma)^2},$$

$$M_2 = -\widehat{\chi}_\parallel\beta\frac{(\gamma-1)/\gamma}{(1-\beta)^2 + \widehat{\chi}_\parallel^2(1-\beta/\gamma)^2},$$

$\gamma = 3$, $c_s^2 = \gamma T/m$, $\beta = c_s^2/v_A^2$, and $\widehat{\chi}_\parallel = (8\beta/\pi\gamma)^{1/2}$ is the parallel heat flux dissipation coefficient which models the intrinsically kinetic effects of resonant particles. Here $\widehat{\mathcal{L}}$ is the resonant particle integral (Hilbert) operator:

$$\widehat{\mathcal{L}}[f](x) = \frac{1}{\pi}\int_{-\infty}^{\infty}\frac{\mathcal{P}}{x'-x}f(x')\mathrm{d}x' \doteq i\frac{k}{|k|}f_k. \quad (7)$$

The sign $\doteq$ denotes equivalence to a Fourier image and $\mathcal{P}$ denotes a principal value integral.

It is interesting first to investigate the influence of Landau damping on a (previously) stable envelope soliton wave train. Figs. 3a-3e depict the KNLS waveforms, hodographs, spectra at different times as well as wave energy degradation and a snapshot of fluctuating fields b_x and b_y at $\tau = 25$ for a soliton initial profile in $\beta = 1$ plasma (i.e. $M_1 = 1.5$, $M_2 = -1.63$). The effect of the collisionless dissipation is apparent from the decreasing amplitude and increasing width of the waveform (Fig. 3a). Energy "inverse cascades" and accumulates in large scales (low-k harmonics), as shown in Fig. 3c. Note that the temporal energy evolution can be separated into two phases (see Fig. 3d), namely a period of rapid damping $0 \leq \tau \leq 5$ (so that $0 \leq t \leq 10^3 \Omega_i^{-1}$) associated with drastic spectral modification, followed by an extended quasi-stationary period (of duration of, at least, $10^4 \Omega_i^{-1}$) during which the energy of the waveform decays very slowly.

The time evolution of an initially linearly polarized parallel propagating wave for the same plasma parameters is shown in Figs. 4. Fig. 4a depicts wave amplitude profiles for four times $\tau = 0, 1, 5, 40$. Localized *quasi-stationary* structures are seen to form very rapidly, the formation time is $\tau_f \sim 2$. Again, the amplitude decreases and the width of the structures increases with time, due to dissipation. Fig. 4b represents the phase portrait of the structures at times $\tau = 1, 5, 40$. The dissipative structures exhibit an easily distinguishable *"S-shaped"* diagram. It is worth to mention that this characteristic shape is well preserved for a wide range of plasma parameters and may be considered a signature of (collisionless) damping (see also Section IV). The harmonic spectrum of the dissipative structures is *narrow*, with most energy associated with *low-k* harmonics (Fig. 4c). For example, for $\tau = 40$ the harmonic tail is almost negligible after $|k| \simeq 10$. Energy decay is shown in Fig. 4d. No distinct phases are seen.

Figs. 5 show the observed localized structures at $\tau = 15$ in more detail. It is seen (Figs. 5a and 5b) that regions of significant field variations are accompanied by fast phase rotation through (approximately) π radians. However, in the regions of negligibly varying $|b|$, linear polarization is preserved. This is easily seen from comparison of Figs. 5b and 5d. At the discontinuity (path A-B-C) the magnetic field vector completes a rotation through π radians (Fig. 5d). During the subsequent quescent region (path C-D), the magnetic field vector resides at the "tip" of the left arm indicating pure linear polarization. At the next discontinuity the vector returns to the initial position, similarly completing a π radian rotation, as shown by dashed path in Fig. 5d. Thus, the KNLS dissipative structures have the requisite properties to be identified as localized, *rotational/directional discontinuities*, as recently observed in the solar wind [22,23]. Note, however, these KNLS rotational discontinuities are associated with the regions of *varying* $|b|$, unlike the conventional definition that $|b| = const$ across the rotational discontinuity. It may be seen from comparison with other cases below that there is no sharp difference between a rotational and directional discontinuity. One may be transformed into another by changing the initial wave polarization and propagation angle. Hence, we use both words to denote the S-type KNLS discontinuity. We should also note the remarkable similarity of hodographs obtained by solution of the KNLS equation and from full numerical plasma simulations [11]. We emphasize the quasi-stationary character of the KNLS discontinuities, with waveform shape preserved for thousands of cyclotron times. The structures exhibit narrow, localized spectra (Fig. 5c). The inverse spectrum width defines the spatial localization of the discontinuity. Also, the small-scale parasitic oscillations typical of the fluid DNLS are absent (they are probably inhibited by Landau damping at earlier stages of evolution). Such KNLS discontinuities occur commonly and are not restricted to β's close to unity. These structures are quite evident in a wide interval of β, of approximately 0.5-0.6 to 1.4-1.6. The formation time increases from $\tau_f \sim 2$ at $\beta \simeq 1$ to $\tau_f \sim 15$ at the ends of the interval. Thus, the dissipative structures still form at smaller M_2, however the formation time increases when M_2 decreases. Wave profiles and spectra still look like those in Figs. 4, 5. The phase diagram, however, changes. Its central part expands and the "arms" become thicker, so that the whole diagram become similar to that shown in Fig. 17d for the case of collisional dissipation. In all cases the phase discontinuity is localized at the discontinuity of $|b|$.

In Figs. 6 the corresponding waveform dynamics for an initially circularly polarized wave with sinusoidal amplitude modulation is shown for the same plasma parameters. In contrast to the previous case, circularly polarized waves do not evolve into structures with discontinuities (smooth, wave-like forms emerge). Rather, they evolve in a few τ to a single (almost purely) circularly polarized harmonic at the lowest k (Figs. 6b, 6c). A smooth, almost negligible amplitude modulation is imposed on the wave. At these regions, weak, arc-polarized phase irregularities occur (see Fig. 6b,e). Such phase irregularities are intermittent structures living just few τ, they carry little energy (which is mostly in higher-k harmonics) and, thus, disappear quickly. Energy decay (Fig. 6e) is substantial during the time of spectrum modification, and extremely slow at later times.

Figs. 7 depict the evolution of an initially elliptically polarized wave, an intermediate case between purely circular and linear polarizations. Plasma parameters are the same as in the previous cases. An elliptically polarized wave evolves to a wave structure of slowly varying amplitude (similar to the circular polarization case) as shown in Fig. 7a. However, there are sudden phase jumps (by π radians) which are localized at regions of varying wave amplitude (typical of linear polarizations). These phase discontinuities (which are the semi-circles in Fig. 7b) are separated by extended regions of linear polarization during which a tip of the magnetic field vector resides at small arms on the graph. Unlike the linear polarization

case, the phase discontinuity is not accompanied by the wave amplitude discontinuity. A harmonic spectrum is again sufficiently narrow and most energy is associated with large scales (see Fig. 7c). Energy dissipation is weak in comparison to linear polarizations (Fig. 7d).

Obliquely propagating waves are still described by the KNLS equation. However, a new wave field which (formally) contains a perpendicular projection component of the ambient magnetic field should be introduced. Assuming the ambient field lies in x-z-plane, we write the new field as

$$b = (b_x + B_0 \sin \Theta + ib_y)/B_0. \qquad (8)$$

The nonlinear evolution of the linearly and highly elliptically polarized waves is strongly sensitive to the angle between the polarization plane and the plane defined by the ambient magnetic field vector and the direction of wave propagation. This angle is set by initial conditions. When this angle is small, the oscillating wave magnetic field has a longitudinal component along the ambient field. Thus, we refer such waves to as *longitudinal*. In the opposite case, the wave magnetic field oscillates (nearly) perpendicularly to the ambient field. Thus, such waves are called *transverse*. Note that classification fails for circularly polarized waves, since a polarization plane cannot be defied in this case.

The time evolution of a transverse wave of initial linear polarization is shown in Fig. 8, for the same plasma parameters and $\Theta = 45°$. Of course, such a value is near the boundary of applicability of the KNLS. However, we run such an exaggerated case because (i) it takes less computer time, as the nonlinear evolution is faster and, thus, (ii) it looks more illustrative than those with smaller Θ. No significant physics is lost, anyway. The wave profiles evolve into two KNLS rotational discontinuities (as in the parallel propagation case) with the typical "S-polarization" in a few τ (see Figs. 8a and 8b). These discontinuities have different group velocities, so some time later ($\tau \sim 15$) they start to interact with each other, as seen in Fig. 8c. Since these discontinuities are characterized by opposite phase rotations, they nearly totally annihilate one another duting the interaction. The final, residual structure has small amplitude ($b/B_0 \simeq 0.1$), and is roughly arc-polarized, as seen in Fig. 8d at $\tau = 30$. This final state is extremely weakly damped (see Fig. 8f) because of the very small magnetic field perturbation amplitude of the waveform (damping in KNLS is nonlinear!). Note here that due to redefinition of the wave field, Eq. (8), the energy formally reads as $E = E_{wave} + (\sin \Theta)^2$, where the last term is not associated with a wave, but is just a new energy zero-level due to the nonzero perpendicular component of the ambient field. The harmonic spectrum evolution is shown in Fig. 8e.

Figs. 9 show the evolution of an obliquely propagating, amplitude modulated, circularly polarized wave for the same conditions. Although some localized structures emerge, they are *not* connected to phase discontinuities. Nevertheless, they have different group velocities and interact (like in the case of a linear polarization) to yield a weakly damped, small amplitude, quasi-stationary, purely arc-polarized waveform (Fig. 9b). The amplitude of the waveform is sufficiently small ($b/B_0 \simeq 0.2$), but larger than for linear polarization (note that $|b|/B_0 \simeq const$ for such a waveform, as seen from Fig. 9a). Such arc-polarized structures seem very similar to those recently observed in the solar wind and identified with arc-polarized rotational discontinuities [24]. We emphasize the almost dissipationless character of such discontinuities (Fig. 9d), inspite of their significant harmonic energy content, as seen from the broad spectrum in Figs. 9c, 10e. The energy evolution of oblique circularly polarized waves (unlike all other cases) exhibits three different stages (see Fig. 9d): (i) the primary spectrum modification when two spatially localized wave structures emerge ($\tau \leq 10$), (ii) interaction of these localized wave structures ($10 \leq \tau \leq 30$), and (iii) formation of a residual arc-polarized rotational discontinuity ($\tau \geq 30$). The different stages of spectrum evolution is also shown in Fig. 9c.

A (quasi-) stationary, arc-polarized discontinuity is shown in details in Figs. 10, for $\tau = 40$. The discontinuity is associated with minor (almost negligible) amplitude modulation (Fig. 10b). As seen from Figs. 10a,b,d, the discontinuity is a localized structure of typically a dispersion width ($\sim v_A/\Omega_i$). The magnetic field vector makes fast clockwise rotation (see the phase diagram, Fig. 10d) through slightly less than π radians (path A-B-C). The ends A and C are connected by a part of circularly polarized wave packet (slow counterclockwise rotation in the phase diagram, along the perfect arc C-D-A). Circular polarization is indicated by smoothly decreasing phase outside the discontinuity (Fig. 10a). Since $|b|^2 \simeq const$ across the discontinuity (as well as for a pure circular harmonic), it is nearly decoupled from dissipation (note, $\widehat{\mathcal{L}}[const] = 0$, and the second [dissipative] term in the KNLS vanishes identically). The harmonic spectrum of the discontinuity depicted in Fig. 10e is quite narrow and of low amplitude (remember, the b_0 harmonic corresponds to the ambient field, not the wave). Note the remarkable similarity of this solution of the KNLS equation to the structures detected in the solar wind and observed in computer simulations [24,13].

The time evolution of an elliptically polarized, obliquely propagating, longitudinal wave (not shown) is very similar to the case of parallel propagation until large times (i.e. $\tau \sim 60$). At later times ($\tau > 60$), an arc-polarized rotational discontinuity forms. There the magnetic field vector rotates rapidly rotation through an angle of less than π radians.

The nonliear evolution of the transverse waves is complitely differennt form that of the longitudinal waves, as shown in Figs. 11. Such waves quickly evolve (i a few τ) to an arc-polarized rotational discontinuity (Fig. 11a,b).

The magnetic field vector rotates through an angle less than 180° at the discontinuity. Energy dissipation is negligible in this case (Fig. 11d). Harmonic spectra of these wveforms are broad (Fig. 11c)

B. The two mode coupling model

To *qualitatively* understand the physical processes which underly the behavior of dissipative nonlinear Alfvén waves (of linear and elliptical polarization), we construct a simple two-mode coupling model. We assume the spectrum consists of three low-k harmonics $k = 0, \pm 1$ (a finite amplitude $k = 0$ harmonic corresponds to oblique propagation, $b_0 = B_\perp/B_0 = \sin\Theta$. This model is based on the results of numerical solutions which show that only two (initially excited) $k = \pm 1$ harmonics dominate the spectra. Other higher-k spectrum components are of relatively small amplitude and thus can be neglected. We also neglect linear dispersion which is significant at the steep fronts, i.e. for broad spectra, only. Here we emphasize once again that we do not pretend to give a quantitatively correct answer, but only intend to get some insight into the essential physics.

We write the wave magnetic field in the form $b = b_+ e^{i\zeta} + b_0 + b_- e^{-i\zeta}$ and substitute it into the KNLS equation, Eq. (3), together with Eq. (6). The system of evolution equations for each harmonic b_j is

$$\dot{b}_+ + 2i(M_1 + iM_2)\left[|b_0|^2(b_+ + b_-^*) + b_+|b_-|^2\right] = 0, \quad (9a)$$

$$\dot{b}_0 = 0, \quad (9b)$$

$$\dot{b}_- - 2i(M_1 - iM_2)\left[|b_0|^2(b_+^* + b_-) + |b_+|^2 b_-\right] = 0. \quad (9c)$$

We first consider the case of parallelly propagating waves, so that $b_0 = \sin\Theta = 0$. The solution of the second equation is simply $b_0 = const$. Dividing the first equation by the third, we obtain the useful equation

$$\frac{db_+}{db_-} = -\frac{(M_1 + iM_2)}{(M_1 - iM_2)}\frac{b_-^*}{b_+^*}. \quad (10)$$

While a general solution can be found, we separately consider (for simplicity) the cases $M_1 = 0$ and $M_2 = 0$.

1. No dissipation, $M_2 = 0$

In the dissipationless (fluid DNLS) limit (i.e. $\beta \to 0$), we have from Eq. (10)

$$|b_+(\tau)|^2 + |b_-(\tau)|^2 \equiv E_* = const \quad (11)$$

which is just conservation of energy. The energy E_* is defined by an initial condition. Using Eq. (11), the system of Eqs. (9a)-(9c) can be easily integrated to yield

$$b_\pm(\tau) = b_\pm(0) \, e^{\mp i\omega_\pm \tau}, \quad (12)$$

where $\omega_\pm = 2M_1|b_\mp(0)|^2 \sim M_1 E_*$. This solution represents resonant energy exchange between the two harmonics. The typical time scale is of order of the shock formation time and is approximately equal to

$$\tau_s \sim (M_1 E_*)^{-1}. \quad (13)$$

2. Strong damping, $M_1 \ll M_2$

In the case of strong damping (i.e. $\beta \simeq 1$), we neglect by the term M_1. Then Eq. (10) yields

$$|b_+(\tau)|^2 - |b_-(\tau)|^2 \equiv \Delta = const. \quad (11')$$

Unlike the previous case, Landau damping conserves the energy difference associated with different Fourier harmonics, so that the $+k \to -k$ symmetry of the spectrum is preserved. Integration of Eqs. (9a)-(9c) with Eq. (11') results in ($\Delta \neq 0$)

$$|b_+(\tau)|^2 = |b_+(0)|^2\frac{\Delta}{(1 + \Delta/|b_+(0)|^2)\exp(8|M_2\Delta|\tau) - 1} \quad (14a)$$

and ($\Delta \to 0$)

$$|b_+(\tau)|^2 = \frac{|b_+(0)|^2}{1 + 8|M_2|\tau}. \quad (14b)$$

Initially elliptical polarizations correspond to $b_+ \neq b_-$, thus

$$|\Delta| = \left||b_+(0)|^2 - |b_-(0)|^2\right| > 0.$$

Thus, harmonic amplitudes decay exponentially at larger times,

$$b_\pm \propto e^{-4|M_2\Delta|\tau} \quad (15)$$

on the characteristic decay time scale of

$$\tau_{decay}^{ell} \sim |M_2\Delta|^{-1} \quad (16)$$

By contrast, initially linear polarizations with $b_+ \simeq b_-$ (i.e. $\Delta \to 0$) decay as a square root of time,

$$b_\pm \propto 1/\sqrt{|M_2|\tau} \quad (15')$$

with the faster characteristic time-scale

$$\tau_{decay}^{lin} \sim |M_2|^{-1} \quad (16')$$

3. Quasi-perpendicular propagation

Now we neglect cubic terms $b_\pm|b_\mp|^2$ in Eqs. (9a)-(9c) as small compared to $b_\pm|b_0|^2 \simeq b_\pm$. Then these equations read

$$\dot{b}_+ + 2i(M_1 + iM_2)|b_0|^2(b_+ + b_-^*) = 0, \qquad (17a)$$

$$\dot{b}_- - 2i(M_1 - iM_2)|b_0|^2(b_+^* + b_-) = 0. \qquad (17b)$$

These yield:

$$\frac{d}{d\tau}(b_+ + b_-^*) + 4i(M_1 + iM_2)(b_+ + b_-^*)|b_0|^2 = 0. \quad (18)$$

It is easily seen that harmonic amplitudes decay exponentially

$$b_\pm \propto e^{-4|M_2|\sin^2\Theta\tau} \qquad (19)$$

and the characteristic decay time is

$$\tau_{decay}^{obl} \sim |M_2 \sin^2\Theta|^{-1} \le \tau_{decay}^{lin} \ll \tau_{decay}^{ell} \qquad (20)$$

Thus, given an isotropic initial distribution, wave excitation in the quasi-parallel direction is most robust while waves in the quasi-perpendicular direction are quickly damped.

Figs. 12 represent the time evolution of two $k = \pm 1$ harmonics for the cases shown in Figs. 4, 7, and 9, respectively. Fig. 12a corresponds to linear polarization (i.e. $\Delta = 0$). The harmonics coincide all the time and decay according to $\sim 1/\sqrt{\tau}$. Fig. 12b is the case of elliptical polarization ($|\Delta| = 0.4$). As seen from this figure, Δ is approximately constant and the harmonics decay exponentially, contrary to the case of linear polarization. Fig. 12c shows the case of obliquely ($\Theta = 45°$) propagating, circularly polarized waves.

Amplitude modulated, parallel propagating circularly polarized waves with initially excited harmonics -1 and -2 can be considered analogously. However, one should consider a spectrum which includes $-2 \le k \le +2$ components. This complicates the analytical treatment of the problem. The characteristic time, however, can be estimated from the elliptical polarization case, Eq. (16). Now $\Delta \simeq |b_{-2}|^2$, and the second (i.e. b_{-2}) harmonic dissipates in a time

$$\tau_{decay}^{circ} \sim \left(|M_2||b_{-2}|^2\right)^{-1}. \qquad (21)$$

After this time, only one b_- harmonic survives. Thus, no significant damping occures.

C. Discussion

The sharp contrast between the nonlinear evolution of initially linearly (elliptically) and circularly polarized parallel propagating wave trains is an immediate consequence of the unique harmonic scaling of collisionless

(Landau) dissipation in the KNLS equation. Integration of Eq. (1) with U_{NL} defined by Eq. (6) over all space (assuming that b vanishes at infinity) yields (in dimensionless variables)

$$\frac{\partial E}{\partial \tau} = -M_2 \int_{-\infty}^{\infty} |b|^2 \frac{\partial}{\partial\zeta} \widehat{\mathcal{L}}\left[|b|^2\right] d\zeta$$

$$= -M_2 \int_{-\infty}^{\infty} \left(\frac{1}{2\pi} \int_{-\infty}^{\infty} e^{ik'\zeta} \left(|b|^2\right)_{k'} dk'\right)$$

$$\cdot \frac{\partial}{\partial\zeta} \left(\int_{-\infty}^{\infty} e^{ik''\zeta} i\frac{k''}{|k''|} \left(|b|^2\right)_{k''} dk''\right) d\zeta$$

$$= \frac{M_2}{2} \int_{-\infty}^{\infty} \left|\left(|b|^2\right)_k\right|^2 |k| \, dk , \qquad (22)$$

where $E = \int_{-\infty}^{\infty} |b|^2 d\zeta$ is the total wave energy, and we assumed $\langle|b|^2\rangle = 0$.(This result have been reported also in Refs. [32,28].) Thus, the rate of energy dissipation is controlled by the coupling coefficient, $M_2 < 0$. Also, we conclude that higher-k harmonics are strongly damped which is typical for a phase-mixing process (i.e. smaller scales mix faster). It is crucial, however, to understand that *collisionless damping enters at all k*, in contrast to hydrodynamic systems where diffusion (viscosity) yields dissipation only at large k (i.e. small scales, or steep gradient regions). Hence, competition of nonlinear harmonic generation (i.e. front steepening) and collisionless damping produces a quasi-stationary energy spectrum which is a *rapidly* decreasing function of k, with the long-time asymptotic behavior dominated by a few low-k harmonics. Since linear polarizations have (initial) spectra symmetric upon $k \to -k$, they couple more strongly to dissipation than circular polarizations do. Moreover, interaction of finite amplitude spectrum components necessarily leads to higher-k harmonic generation and wave steepening. Such interactions are excluded for pure circular polarization. Therefore, the circularly polarized wave evolves to a single harmonic final state, which is, itself, a stationary (and exact) solution of the KNLS equation (i.e. it experiences no steepening and minimal damping).

Since Landau damping enters symmetrically for $+k$ and $-k$ spectrum components, it does not change the initial symmetry of a spectrum, so that the sense of an initial polarization (set by initial spectrum symmetry) is preserved (neglecting feeble high-k, low-amplitude asymmetry induced by steepening). Thus, KNLS evolution preserves initial wave helicities forming directional/rotational discontinuities at the edges of the regions of linear (elliptical) polarization. These directional/rotational discontinuities are localized at regions of strong amplitude variations, unlike the conventional view [1] where the shock and rotational discontinuity are well separated and have different group velocities. The KNLS directional/rotational discontinuities display a well distinguished S-shaped phase portrait which can be considered a footprint of the occurrence of strong Landau damping in satellite observations. Since the KNLS

equation preserves (initial) wave helicity [30,31] , rotational discontinuities do not form from circularly polarized waves. Given that circular polarizations decay much more slowly than linear polarizations do, the results suggest that large-scale circularly polarized waves should occur more frequently than small scale discontinuities which evolve from linear polarizations (given comparable initial populations), especially at large distances from the Sun.

Oblique and quasi-perpendicular, linearly polarized waves first evolve to two KNLS directional/rotational discontinuities of opposite phase rotation propagating with different group velocities, so that they finally merge and annihilate to yield weakly-nonlinear, small amplitude, arc-polarized waves. Despite the fact that oblique, circularly polarized waves do not form KNLS rotational discontinuities, their final state is similar to (but of larger amplitude than) that of a linear polarization. Since, oblique and quasi-perpendicular (both linear and circular polarizations) waves are coupled to the ambient magnetic field $B_\perp = B_0 \sin \Theta$, which is usually (much) larger than the fluctuating wave field b, the process of energy dissipation is $B_\perp^2 / b^2$ times faster for such waves. Waveforms again evolve to the lowest-k state which is now the single harmonic $b_0 = B_\perp / B_0$ (which corresponds to the ambient field component, not the wave perturbed field) indicating dissipation of *all wave energy*. Thus, the final state of nonlinear evolution for "off-axis" propagating waves is a (very) small amplitude, weakly-nonlinear, *weakly-damped*, arc-polarized Alfvén wave packet. Pure arc-polarized waveforms (which develop from circular polarizations) have much in common with the structures recently observed in the solar wind and identified with arc-polarized rotational discontinuities [24]. Such structures experience minimal damping. The comparably fast damping of oblique and quasi-perpendicular waves suggests that most magnetic fluctuations should occur at small angles to the ambient field (given initial isotropic fluctuations) resulting in large turbulence levels in parallel and quasi-parallel directions and small turbulence levels in quasi-perpendicular directions where Alfvénic turbulence is sufficiently suppressed.

IV. COLLISIONAL DISSIPATIVE ALFVÉN TRAINS

A. Numerical solutions

The evolution equation for coherent Alfvén waves is again Eq. (1) with the nonlinear velocity perturbation term written as

$$U_{NL} = \frac{v_A}{2} \left\{ Q_1 \left(|b|^2 - \langle |b|^2 \rangle \right) + Q_2 \widehat{\mathcal{J}}_L \left[|b|^2 - \langle |b|^2 \rangle \right] \right\},$$

(23)

where

$$Q_1 = \frac{1}{(1 - \beta/\gamma)},$$
$$Q_2 = -\frac{\beta}{\chi_\parallel^c} \frac{\gamma - 1}{\gamma} \frac{1}{(1 - \beta/\gamma)^2},$$

$\gamma = 3$, and $\chi_\parallel^c$ is the parallel heat conduction coefficient which represents diffusive (collisional) energy dissipation. Here $\widehat{\mathcal{J}}_L$ is the collisional dissipation (integral) operator

$$\widehat{\mathcal{J}}_L[f](x) = e^{-x/L} \int^x e^{x'/L} f(x') \mathrm{d}x' \doteq \frac{1}{1/L - ik}, \quad (24)$$

where $L = (\chi_\parallel^c / v_A)(1 - \beta/\gamma)/(1 - \beta)$. For future use we introduce $\kappa = \bar{z}/L$, the dimensionless dissipation scale, i.e. the ratio of a typical wave length to the dissipation length. For β close to unity we may write approximately $\kappa \simeq [75(1 - \beta)/\chi_\parallel^c](v_A^2/\Omega_i)$.

As in the case of collisionless dissipation, we first investigate the temporal evolution of an (initially) soliton wave envelope, Eqs. (5a)-(5b), since it is stable in absence of any dissipation. Solutions at different times are shown in Figs. 13 with $\kappa = 100$ and $\beta = 0.99$. We shall see that collisional dissipation is strongest when $\kappa \sim k$, i.e. when the dissipation scale is comparable with a typical wave-length of a train. We again (as with Landau damping) see rapid primary spectrum and spatial profile modification (Figs. 13c,a, respectively) and formation of a quasi-stationary solution with negligible energy degradation (Fig. 13d). The hodographs are shown at three times $\tau = 0, 4, 25$ in Fig. 13b. The steady-state profiles of b_x and b_y are shown separately in Fig. 13e. We should mention that the effect of collisional damping is significant only for β very close to unity.

The nonlinear evolution of an initially linear polarization (in $\beta = 0.99$ plasma) is shown in Figs. 14, 15, 16 for weakly collisional ($\kappa = 200$), intermediate ($\kappa = 20$), and strongly collisional ($\kappa = 2$) regimes, respectively. Energy dissipation is represented in Figs. 18. In a weakly collisional regime (Figs. 14), a wave experiences steepening of the back front, as a result of nonlinear dispersion set by the sign of κ (or L) which, in turn, depends on plasma β. Since the nonlinear dispersion is positive in this case, it competes with the linear (negative) dispersion. The nonlinear dispersion is most important in regions of a high wave magnetic field (since it is proportional to $|b|^3$), while conventional linear dispersion [last term in Eq. (1)] is important where $|b|$ is small. Parasitic small-scale circularly polarized oscillations appear on the steep fronts when wave steepening is limited by dispersion (Figs. 14a,b). These parasitic harmonics, however, disappear quickly as a consequence of the fact that high-k components are strongly coupled to dissipation. The magnetic field vector rotates rapidly at the steepened edge of the wave. After the phase of nonlinear steepening, a propagating shock wave separates from the (standing) phase rotation region (i.e. the rotational discontinuity). The width of the shock front is controlled by collision length L and

its amplitude gradually decreases due to damping (Fig. 14c). Such a process is remarkably similar to that first discussed by Cohen and Kulsrud [1]. However, it is just one limiting case ($\kappa \to \infty$) of the KNLS wave evolution. The spatial width of the rotational discontinuities is controlled by dispersion. Hodographs of rotational discontinuities presented in Fig. 14d are different from the Cohen-Kulsrud case. Here the magnetic field vector b makes a counterclockwise rotation through some angle (typically $50° - 90°$) and than makes a clockwise rotation to complete a total $180°$ phase jump across the discontinuity. As shown in Fig. 14e, harmonic spectra are broad, as collisional damping enters at small scales $k \geq \kappa$.

Figs. 15 correspond to intermediate collisional damping ($\kappa = 20$). Parasitic small-scale, small amplitude oscillations are still emitted from the seepened front (Fig. 15a,b). Propagating shocks (Fig. 15c) are sufficiently broad and disappear at a higher rate than those in the weakly collisional case. Rotational discontinuities are localized at the regions of significant amplitude $|b|$ variations, and the typical hodograph takes on an S-shape (however, with "inflated", almost semicircular central part). The harmonic spectrum is narrower than in the $\kappa = 200$ case (Fig. 15e). The rotational discontinuities move slowly to the right (as with Landau dissipation). Neither the sign of κ, nor the direction of shock wave propagation affect the propagation direction of these phase discontinuities. More details of this case are shown in Figs. 17 at $\tau = 15$. A remarkable similarity of these figures to those of Figs. 5 (Landau damping case) indicates a lack of a characteristic dissipation scale in the system, i.e. the dissipation scale is comparable with a typical wave-length, $\kappa \sim k$.

The strong collisional regime is represented in Figs. 16. This case exactly corresponds to that with Landau damping, since collisional and wave lengths are equal (note, the k-scaling of damping is different). No small-scale harmonics emerge, and shock wave generation is suppressed by damping (Fig. 16a), as typical of Landau dissipation S-shaped hodograph displays (Fig. 16b). Most of the energy is located in a few low-k harmonics (Fig. 16c). For a more strongly collisional regime ($\kappa = 0.2$, results are not shown) the effect of dissipation becomes weaker, and wave evolution becomes similar to that of the weakly damped wave case. This effect is associated with the weakness of the resonant coupling (defined by Q_2 coefficient) of Alfvén and ion-acoustic waves.

The temporal evolution of wave energy is shown in Fig. 18a for several collisional regimes, from weak collisionality ($\kappa = 200$) to a collision dominated plasma ($\kappa = 0.2$). Fig. 18b depicts total wave energy content as a function of κ [i.e. heat conduction coefficient as $(\chi_\parallel^c)^{-1}$] at different times $\tau = 5, 10, 20$. The energy dissipation rate increases with collisionality (i.e. with decrease of κ) until $\kappa \sim 1$ and decreases for $\kappa < 1$. The last effect is due to the weak coupling of Alfvén and ion-acoustic waves (the coefficient Q_2), which occures when the ion-acoustic

frequency becomes smaller than its collisional damping rate.

Since the sign of κ (or L) defines the sign of nonlinear dispersion, we also considered the case of $\beta > 1$. Traces of typical evolution are depicted in Fig. 19 for $\kappa = -20$ and $\beta = 1.01$. In this case both linear and nonlinear dispersions are negative (and do not compete), so many small scale oscillations appear at the (sharp) front of a wave train (Fig. 19a,b). This " noisy" harmonic generation is possibly related to the modulation instability of steep fronts against small-scale modulations [14]. The instability growth rate in the collisionless regime decreases with increasing wave amplitude. In the collisional regime, the growth rate is amplitude independent. Thus, the large amplitude suppression which is the case for collisionless damping is absent for diffusively dissipative Alfvén waves. Further evolution of Alfvén trains generally follows the previous cases where $\beta < 1$.

Circular polarizations evolve similarly to the Landau damping case. Despite the emergence of a shock wave (especially in a weakly collisional plasma), they do not evolve to rotational discontinuities. Instead, they generate smooth waveforms with irregular phase rotation. The sign of κ again defines the sign of dispersion. Its value controls spatial scales. The result of dissipative evolution is a dominant (lowest-k), circular harmonic and a low-amplitude harmonic background tail, spreading up to scales $k \sim \kappa$. For illustration, Figs. 20 show evolution of a circularly polarized wave in a weakly dissipative plasma (more typical for astrophysical situations) with $\beta = 0.99$ and $\kappa = 200$.

B. Discussion

A significant difference between collisional (diffusive) and collisionless (Landau) dissipation is the existence of a characteristic collisional scale for the former case. As usual, it represents a "boundary" between the weakly and the strongly damped (i.e. low and high-k, respectively) parts of wave spectra. Integrating Eq. (1) with U_{NL} from Eq. (23) over space (see Section III), we obtain:

$$\frac{\partial E}{\partial \tau} = -Q_2 \int_{-\infty}^{\infty} \left(\widehat{\mathcal{J}}_L \left[|b|^2 \right] \frac{\partial}{\partial \zeta} |b|^2 + 2|b|^2 \frac{\partial}{\partial \zeta} \widehat{\mathcal{J}}_L \left[|b|^2 \right] \right) d\zeta$$
$$= \frac{Q_2}{2} \int_{-\infty}^{\infty} \left| (|b|^2)_k \right|^2 \frac{ik}{L^{-1} - ik} \, dk$$
$$= Q_2 \int_0^{\infty} \left| (|b|^2)_k \right|^2 \frac{k^2}{\kappa^2 + k^2} \, dk \; . \tag{25}$$

Thus, energy dissipation is controlled by both the coefficient $Q_2 < 0$ (which, in turn, controls the coupling of the Alfvénic mode to the damped ion-acoustic mode), and the dissipation scale $\kappa \propto (1 - \beta)/\chi_\parallel^c$. Unlike the collisionless case, diffusion enters at particular scales $k \geq \kappa$. As a result, shock waves may form and their steepening will be limited by the collisional scale κ. The sign

of κ defines the sign of nonlinear dispersion (e.g. steepening direction, etc.) and does not affect the dissipation rate. Since most spectral energy is associated with sufficiently small-k components, the integral in Eq. (25) increases with decreasing κ until κ is about unity. For smaller κ the integral is approximately constant. The coupling coefficient Q_2 decreases with decreasing κ (for constant β). The higher the plasma collisionality, the weaker the resonance of Alfvén and ion-acoustic waves, and thus the smaller Q_2 is. Thus, the energy dissipation rate is *maximum* when the dissipation length is comparable with a typical wave-length. For a strongly collisional regime, ion-acoustic wave damping rate becomes larger than its frequency, so that ion-acoustic perturbations are no longer a plasma eigenmode. Resonant coupling and energy transfer from an Alfvénic mode to ion-acoustic oscillations is weak, despite strong dissipation of the latter.

One may mention the interesting case of strong damping ($\kappa \simeq \lambda_{wave}^{-1}$). In this case, the system evolves as if subject to collisionless dissipation, i.e. S-polarized KNLS dissipative structures emerge from linear polarizations and circular polarizations quickly evolve to a single harmonic state. However, such a scale-free regime may occur only in strongly collisional plasma, $\chi_{\parallel}^c \geq v_A^2/\Omega_i$, with β very close to unity ($0.95 \leq \beta \leq 1.05$). Inspite of its rare occurrence in nature, this case allows us to understand physical the reasons underlying the uniqueness of collisionless (Landau) dissipation for Alfvén wave dynamics.

The weakly collisional regime ($\kappa \to \infty$) seems more typical for astrophysical and space plasmas. Nonlinear steepening of a wave front is first limited by nonlinear dispersion, giving rise to radiation of small-scale, circularly polarized, noisy parasitic oscillations by the steep front (probably due to modulational instability). These oscillations damp quickly. At later times, the front separates into a shock wave moving in the direction of primary wave steepening and a waveform the type of which (e.g. directional or rotational discontinuity, small-scale phase modulations, etc.) depends on the initial wave polarization. For initially linear polarizations, this waveform is a rotational discontinuity (with a weak amplitude modulation imposed on it). For circular polarizations, it is an intermittent, wavy structure (the amplitude of perturbations of $|b|$ decreases with time), carrying weak, roughly arc-polarized phase irregularities. The rotational discontinuity (for $\beta < 1$) consists of partially counterclockwise rotation through some angle (typically $50° - 90°$) followed by clockwise rotation through an angle larger than $180°$ to complete a $180°$ phase difference across the discontinuity. These waveforms have a characteristic spatial scale set by dispersion. The propagating shock wave front is much narrower and controlled by collisions. The amplitude of a shock decreases with time due to collisional (diffusive) dissipation. The residual waveforms are weakly coupled to nonlinear dissipation because $|b| \simeq const$ across them. In general, linear polarizations are more strongly damped than circular ones.

Given that both linear and circular polarizations are initially excited, the weakly collisional quasi-stationary turbulence will consist of smooth waveforms associated with rotational discontinuities and purely circularly polarized, high amplitude waves.

Consider again Eq. (25) in a weak collisional regime, i.e. $\chi_{\parallel}^c \to 0$. Then, as $\kappa \propto (1 - \beta)/\chi_{\parallel}^c$, κ is extremely large (and dissipation is very weak) for all values of β, except $\beta \cong 1$. The coefficient $Q_2 \propto \beta/\chi_{\parallel}^c$ is not singular at $\beta = 1$. Thus, for $|\beta - 1| \not\simeq 0$ the dissipation rate $\dot{E} \sim Q_2/\kappa^2 \sim \chi_{\parallel}^c/(1 - \beta)^2 \to 0$, indicating weak wave damping. However, for β close to unity, we infer from Eq. (25) that $\kappa \to 0$ and $\dot{E} \sim Q_2 \sim 1/\chi_{\parallel}^c$ which is *larger*, for *weaker* collisionality. In space plasma, β is a typically decreasing function of the distance from the sun [i.e. $\beta = \beta(R)$], starting from $\beta > 1$ near the sun and decreasing to $\beta < 1$ further from it. Moreover, this plasma is only weakly collisional. According to the discussion above, nonlinear waves propagating out of the sun are extremely strongly damped in a narrow region at the distance R_d where $\beta(R_d) \simeq 1$. This region should be easily identifiable by a (much) higher (electron) temperature compared to elsewhere. The width of the region of enhanced dissipation may be estimated from the condition $\kappa \propto \left[75 \left(1 - \beta(R) \right) / \chi_{\parallel}^c \right] \left(v_A^2/\Omega_i \right) \simeq 1$. Thus, the smaller the collisionality, the thinner the high temperature region. Because of strong damping at $\beta = 1$, waves existing at distances either $R > R_d$ or $R < R_d$ never transit through the point $R = R_d$ which is thus can act as a "sharp boundary" between these two regions. Thus, the level of magnetic field perturbations will be low beyond the point R_d (assuming that the Alfvénic fluctiations have been generated near the sun), provided the width of the dissipation region is large enough.

V. GYRO-KINETIC (FINITE LARMOR RADIUS) EFFECTS ON SLIGHTLY OBLIQUE ALFVÉN TRAINS

A. Numerical solutions

The evolution equation in this case is again Eq. (1). The nonlinear velocity perturbation reads

$$U_{NL} = \frac{v_A}{2} \left\{ \left[\left(M_1 - \frac{N_1}{\Lambda^2} \right) + \left(M_2 - \frac{N_2}{\Lambda^2} \right) \widehat{\mathcal{L}} \right] \right. \tag{26}$$

$$\left. \cdot \frac{\left(\widehat{\mathcal{J}}_\Lambda - \widehat{\mathcal{J}}_{-\Lambda} \right)}{2\Lambda} + \frac{1}{\Lambda^2} \left(N_1 + N_2 \widehat{\mathcal{L}} \right) \right\} \left[|b|^2 - \langle |b|^2 \rangle \right],$$

where

$$\Lambda^2 = -2\eta_{\parallel}^2 \beta \frac{(1 - \beta) + [\widehat{\chi}_{\parallel}^2/\gamma](1 - \beta/\gamma)}{(1 - \beta)^2 + \widehat{\chi}_{\parallel}^2(1 - \beta/\gamma)^2},$$

$$N_1 = \eta_\parallel^2 \frac{(1 - 2\beta) + \widehat{\chi}_\parallel^2 (1 - 2\beta/\gamma)}{(1 - \beta)^2 + \widehat{\chi}_\parallel^2 (1 - \beta/\gamma)^2},$$

$$N_2 = -2\eta_\parallel^2 \widehat{\chi}_\parallel \beta \frac{\gamma - 1}{\gamma} \frac{1}{(1 - \beta)^2 + \widehat{\chi}_\parallel^2 (1 - \beta/\gamma)^2},$$

$\eta_\parallel^2 \equiv (\rho_i^2/2) \sin^2 \Theta$, and ρ_i is the ion gyro-radius. [Eq. (49) of Ref. [14] contains a typographical error, in that the two terms in round brackets were omitted]. Note here that Λ^2 can take on both positive and negative values. The operator $\widehat{\mathcal{L}}$ represents the effects of resonant particles. The operator which contains Larmor averaging is a composition of two collisional operators $\widehat{\mathcal{J}}_L$. It can be written as

$$\frac{1}{2\Lambda} \left(\widehat{\mathcal{J}}_\Lambda - \widehat{\mathcal{J}}_{-\Lambda} \right) \doteq \frac{1}{2} \left(\frac{\kappa}{\kappa - ik} + \frac{\kappa}{\kappa + ik} \right), \qquad (27)$$

where we redefine $\kappa = \bar{z}/\Lambda$. Thus it can assume either real or imaginary values.

In the limits $k\rho_i \ll 1$ and $\Theta \ll 1$ (i.e. $k/\kappa \ll 1$), we may expand denominators in the right hand side and plug into Eq. (26). Then, to lowest order, we write

$$U_{NL} \Big|_{\Lambda \to 0} = \frac{v_A}{2} \Bigg\{ \left(M_1 + M_2 \widehat{\mathcal{L}} \right) + \left[\left(\Lambda^2 M_1 - N_1 \right) \right.$$

$$\left. + \left(\Lambda^2 M_2 - N_2 \right) \widehat{\mathcal{L}} \right] \frac{\partial^2}{\partial \zeta^2} \Bigg\} \left[|b|^2 - \langle |b|^2 \rangle \right]. \quad (28)$$

First, one may notice that there is no sharp transition from the $\Lambda^2 > 0$ regime to the $\Lambda^2 < 0$ regime. Second, gyro-averaging the wave fields results in nonlinear dispersion of waves. It does not introduce additional dissipation. It may, however, generate (due to modulational instability) a large number of strongly damped high-k harmonics. Thus, it may affect the wave damping process.

Figs. 21 and 22 depict the evolution of linearly and circularly polarized initial conditions (respectively) in $\beta < 1$ environment for $\kappa = 3000$ which corresponds to $k\rho_i \simeq 0.08$. The angle of wave propagation is $\Theta = 45°$ in both cases. There is no significant difference observed in the evolution of an oblique linear polarization for zero and finite Larmor radii (compare Figs. 8 and 21, respectively). Quasi-stationary KNLS dissipative structures (i.e. rotational discontinuities with $|b|^2 \neq const$) form during the evolution. The width of each is controlled by both linear and nonlinear (due to gyro-kinetic effects) dispersion. The harmonic spectrum, however, is more irregular than in the case of zero Larmor radius (Fig. 21c). In contrast, an obliquely propagating, circularly polarized wave behaves differently, and its evolution is closer to the parallel propagating case. No arc-polarized structure forms from an initially circular polarization. Only a waveform with dominantly low-k circularly polarized harmonic forms instead (Fig. 22b).

Finite Larmor radius effects enter the energy dissipation rate, as shown in Figs. 23. In this case $\beta = 1.3, \kappa =$

50 (i.e. $k\rho_i \simeq 0.5$), and $\eta = 0.2$. Again, two KNLS rotational discontinuities of opposite senses of polarization form. They interact with each other quickly due to their increased width (set by dispersion), despite the fact that their group velocities are similar. The combined effects of Landau damping and nonlinear Larmor dispersion result in rapid wave energy decay. This is shown in Figs. 23c,d.

We should mention another interesting case (results are not shown). For $\beta < 1$ and comparably small $|\kappa|$ ($\leq 50 - 100$), solutions of the KNLS equation are unstable, i.e. the amplitudes of several harmonics increase rapidly with time. Our program does not allow us to follow the full dynamics of such solutions, because a fast Fourier transform (used in the program) works correctly only when harmonic amplitude vanishes quickly with increasing k. Note however that the perturbative derivation of the KNLS fails in this case, too. The physical understanding of this instability is discussed in the next subsection.

B. Discussion

It is easily seen that finite Larmor radius corrections alone do not introduce a damping process of any kind. Nevertheless, they can change the energy dissipation rate via collisionless damping Indeed, it can even change the sign of the dissipation, as will be discussed later. Using our previous results, namely Eqs. (22) and (25), we may now easily write

$$\frac{\partial E}{\partial \tau} = -\frac{1}{2} \int_{-\infty}^{\infty} \left| (|b|^2)_k \right|^2$$

$$\cdot \left\{ \left(M_2 - \frac{N_2}{\Lambda^2} \right) \frac{\kappa^2}{\kappa^2 + k^2} + \frac{N_2}{\Lambda^2} \right\} |k| \, dk. \qquad (29)$$

It is very important to emphasize that κ^2 is *not* necessarily *positive*, but defined by the value of β (i.e. $\kappa \propto 1/\Lambda$). Thus, the last equation may be rewritten as

$$\frac{\partial E}{\partial \tau} = \begin{cases} \int_0^\infty \left| (|b|^2)_k \right|^2 \\ \quad \cdot \left(M_2 \dfrac{\kappa^2}{\kappa^2 + k^2} + \dfrac{N_2}{\Lambda^2} \dfrac{k^2}{\kappa^2 + k^2} \right) k \, dk, \qquad \kappa^2 > 0; \\[4mm] \int_0^\infty \left| (|b|^2)_k \right|^2 \\ \quad \cdot \left(M_2 \dfrac{|\kappa^2|}{|\kappa^2| - k^2} + \dfrac{N_2}{|\Lambda^2|} \dfrac{k^2}{|\kappa^2| - k^2} \right) k \, dk, \; \kappa^2 < 0. \end{cases}$$

$$(29')$$

Thus, nonlinear Larmor corrections for high-β plasma (i.e. $\kappa^2 > 0$) may result in enhanced dissipation, only. At low-β (i.e. $\beta < 1, \kappa^2 < 0$) they may also change the sign of $\partial E/\partial \tau$ at least for $|k| > |\kappa|$, i.e. result in instability (i.e. pumping of a wave by plasma resonant

particles). In the case of β less than unity, we replace $\kappa \rightarrow -i|\kappa|$ in Eq. (27). It becomes

$$\frac{1}{2i\,|\Lambda|}\left(\widehat{\mathcal{J}}_{i|\Lambda|} - \widehat{\mathcal{J}}_{-i|\Lambda|}\right) \doteq \frac{1}{2}\left(\frac{|\kappa|}{|\kappa| + k} + \frac{|\kappa|}{|\kappa| - k}\right) \quad (30)$$

which reveals singularities of the finite Larmor operator at $\pm k = |\kappa|$. The terms on the right hand side change their signs at $k = \mp|\kappa|$. Thus, the sign of Landau damping ($\propto \widehat{\mathcal{L}}$) changes sign for right hand polarized harmonics with $k < -|\kappa|$ (the first term) and left hand polarized waves with $k > |\kappa|$ (the second term). Most small-k harmonics are damped on bulk plasma resonant particles. Since plasma particles rotate over their Larmor circles (in the perpendicular plane) along with longitudinal thermal motion, some large-k harmonics may experience growth due to cyclotron resonance with the particles from the tail of the distribution function. Thus, finite Larmor radius effects together with the effect of resonant particles in $\beta < 1$ environment can drive an ion-cyclotron instability (for growing harmonics $k > |\kappa|$) as well as ion-cyclotron damping ($k < |\kappa|$), enhanced dissipation (due to nonlinear dispersion) in $\beta > 1$ plasma. Of course, the ion-cyclotron instability saturates with time by, for example, particle distribution function modification, an effect which is not included in this simple model. For some values of plasma parameters, however, conventional Landau damping may overcome generation of harmonics and suppress the instability.

VI. CONCLUSIONS

In this paper, the influence of various kinetic effects (e.g. Landau and diffusive dissipation as well as effects of the gyro-averaging of fluctuating fields on a Larmor radius scale) were investigated in detail. A tractable analytic evolution equation, the KNLS equation, was numerically solved to study nonlinear dynamics of finite-amplitude coherent Alfvén waves in a finite-β, $T_i \simeq T_e$ plasma, natural to the solar wind. Previous DNLS studies failed to describe the evolution of the wide class of discontinuous waveforms which were recently observed in the solar wind. These waveforms are the (i) *arc-polarized* rotational discontinuities with phase difference *less* and *equal* to π and (ii) *S-polarized* rotational and directional discontinuities. Current study shows that *all* these discontinuous wave structures discussed are *distinct solutions* of the same *simple* analytical KNLS model for different initial conditions, e.g. initial wave polarization and wave propagation angle. The results are summarized in Table I.

I. *Collisionless (Landau) damping* introduces a unique *scale invariant* dissipation process into the dynamics of Alfvénic trains. In contrast to viscous/diffusive dissipation, Landau damping is not restricted to small scales. Thus, it is not surprisingly that the harmonic content of collisionless dissipative waveforms tends to be dominated by large scales, with most wave energy contained in the low-k harmonics. Since there is no characterictic dissipation scale in the system, the scale of the disssipative stuctures is set by *dispersion*, alone (*a là* collisionless solitons and shock waves). The dynamics of Alfvén waves is sensitive to their sense of polarization, as well as to their propagation direction with respect to the ambient magnetic field. The principal results are:

1. *(quasi-), parallel initially linearly polarized waves* evolve rapidly to form *dissipative structures* separated by regions of linearly polarized Alfvén waves. These structures, which are naturally quasi-stationary, extend the traditional genre of collisionless shocks to encompass the structures occurred via the competition of harmonic generation (i.e. nonlinear wave steepening) and collisionless (Landau) damping, rather than dispersion (i.e. as for solitons). Such structures are commonly occurring over a wide range of plasma β, roughly: $0.5 \leq \beta \leq 1.5$. These structures are characterized by fast phase changes (phase jumps). Namely, the magnetic field vector rotates first through some angle (typically, $50° - 90°$), followed by rotation in the opposite direction through an angle larger than $180°$ to complete the total π radian phase change. The phase diagram of the wave displays a distinct *S-shape*, which allows us to relate these dissipative structures to a class of S-type directional/rotational discontinuities observed in the solar wind. Unlike conventional rotational discontinuities, for which $|B|^2 = const$, these KNLS rotational/directional discontinuities exhibit significant amplitude variation across the phase jumps. The amplitude of these variations depends on the angle of propagation and is largest for exactly parallel propagation. The KNLS rotational/directional discontinuities have small velocity in the wave frame. Their directions are defined by the sign of the nonlinearity coefficient M_1 (the discontinuity propagates with the wave for $M_2 > 0$). The dissipative character of these structures is revealed by their increasing width and decreasing amplitude. Dissipation is strong in this case, and energy decays roughly as $E(\tau) \propto 1/(|M_2|\tau)$. Since the KNLS directional/rotational discontinuities display a prominent S-shaped phase portrait, they can (potentially) be regarded as a signature of strong Landau damping at work in satellite observations.

2. *(quasi-) parallel, initially circular polarizations* do not form discontinuities. Since Landau damping preserves the initial symmetry of the harmonic spectrum, circular polarizations form intermittent, roughly arc-polarized waveforms which dissipate quickly, yielding purely circularly polarized waves at the lowest k. Such waves experience no nonlinear steepening and minimal damping. The different evolution of linear and circular polarizations is

due to specific coupling of the waves to collisionless damping, which is, in turn, sensitive to the (initial) symmetry of the harmonic spectrum.

3. *(quasi-) parallel, initially elliptically polarized waves* represent an intermediate case between linear and circular polarizations. Well localized, rotational discontinuities (similar to dissipative structures) form. They are separated by large regions of linearly polarized waves. Amplitude variations across the discontinuities are small. These waveforms are more weakly coupled to dissipation. The total energy of the waveforms decays as $E(\tau) \propto \exp(-\Delta|M_2|\tau)$, where $\Delta = |b_{+1}|^2 - |b_{-1}|^2$ is the difference in energy between the two initially excited harmonics.

4. *oblique, initially linearly polarized, longitudinal waves* form KNLS rotational/directional discontinuities (dissipative structures) with opposite phase rotations, having different group velocities. Thus, these wave structures may interact to annihilate each other. As these waves are nonlinearly coupled to the (large) ambient field $B_\perp = B_0 \sin\Theta$, they are connected to dissipation more strongly than quasi-parallel waves are. Thus, the wave energy dissipate rapidly: $E(\tau) \propto \exp(-|M_2|\tau)$. Residual, small-scale, weakly-nonlinear, weakly-damped Alfvénic perturbations may survive for a long time.

5. *oblique, initially circularly polarized waves and elliptically polarized, longitudinal waves* do not generate dissipative structures. Despite this, they evolve to stationary waveforms with negligible amplitude and large phase variations. Their phase diagram displays a pure arc, with the arc-angle less than 180°. Fast magnetic vector rotation along the arc at the discontinuity is followed by a part of an oppositely rotating circularly polarized wave. Thus, these structures have all requisites to be identified with *arc-polarized rotational discontinuities* observed in the solar wind. This waveform experiences *no damping* and nonlinear steepening. However, the energy content of this waveform is not small.

6. *oblique, transverse waves* evolve to stationary *arc-polarized rotational discontinuities* with the arc-angle less than 180°. The energy content of this waveform is large.

According to the discussion above, nonlinear Alfvén waves subject to damping on resonant particles evolve to narrow-spectrum waveforms with most energy concentrated in lowest-k harmonics. The initial spectrum symmetry (i.e. the wave polarization) is generally preserved during the evolution. Based on the above, one can suggest that (given initial equal populations of isotropically distributed circular and linear polarizations) quasi-

parallel magnetic field fluctuations will consist of predominantly circularly polarized waves and lower amplitude S-polarized KNLS directional discontinuities, while oblique perturbations are predominantly arc-polarized discontinuities, separated by pieces of oppositely circularly polarized waves. One should emphasize that *all* wave structures emerge naturally through the nonlinear evolution of simple, sinusoidally amplitude modulated Alfvén waves with no *a priori* assumptions or special initial conditions used.

II. The dynamics of nonlinear Alfvén wave trains subject to *diffusive (collisional) damping* differ significantly. There are two different regimes of weak and strong plasma collisionality, controlled by the ratio of dissipation length L to the typical wavelength λ, i.e. $|L| \ll \lambda$ and $|L| \geq \lambda$, respectively. The results are:

1. The effect of collisions introduces nonlinear dispersion into the dynamics, along with a nonlinear damping process. Thus it affects the direction of steepening, rate of spectrum modification, etc..

2. The sign of L defines the sign of *nonlinear dispersion* which, in turn, is controlled by plasma β, i.e. $L \propto (1 - \beta)$. Thus, for $\beta < 1$ and $\beta > 1$, nonlinear steepening occurs at the rear and front edges of a train, respectively.

3. The absolute value of L affects the *dissipation rate*. The damping rate has a maximum near $|L| \simeq \lambda$. In the weakly collisional regime, the dissipation process is slower on account of infrequent collisions. However in higher collisionality plasma, the acoustic mode is strongly damped, so it is no longer a plasma eigenmode (i.e. $\omega < \gamma$, here γ is the damping rate). Thus, resonant energy transfer from Alfvénic to acoustic waves is suppressed.

4. In a *weakly collisional regime*, a nonlinear wave evolves to a propagating shock wave (the direction of propagation coincides with the direction of wave steepening) and a rotational discontinuity or phase irregularities, depending on an initial polarization, i.e. whether the initial polarization is linear or circular, respectively. The shock amplitude gradually decreases due to damping. The thickness of the shock is controlled by collisions, however the spatial size of the phase discontinuity/irregularities is larger and controlled by dispersion. In a *strongly collisional regime*, the wave evolution is much similar to the case of Landau damping. Obviously, the system lacks the characteristic dissipation scale in this limit, i.e. $|L| \sim \lambda$.

5. The dissipation process is very sensitive (especially in *weakly* collisional plasma) to the value of β, and sharply peaked at β equal to unity. If one assume $\beta = \beta(R)$ is a function of the distance from the sun, then waves generated near the sun and propagating

outward will be strongly damped at the distance R_d defined by $\beta(R_d) = 1$. One can, thus, expect increased plasma temperature in this region, as well as decreased magnetic field fluctuation level (i.e. characteristic amplitude of Alfvén waves) beyond this point, i.e. at distances $R > R_d$. This process may be important, however, when the width of the dissipation region is large enough (comparable to or exceeding the typical wavelength). This is, in turn, controlled by the spatial profile of β.

III. Effects of *finite Larmor radius* impact the dynamics of obliquely propagating waves, only. They are associated with small-scale gyro-averaging of fluctuating fields on a scale of Larmor orbits of plasma particles. These effects

1. introduce *nonlinear dispersion* controlled by the plasma β, Larmor scale ρ_i, and angle of propagation Θ.

2. typically *suppress* the formation of arc-polarized discontinuities from initially circular polarizations, but do not change the qualitative evolution of linear polarizations.

3. affect the wave energy damping rate in high-β plasma ($\beta > 1$) and may even change the sign of the dissipation in low-β plasma ($\beta < 1$). The last case corresponds to an instability. Thus, as a result of gyro-motion of resonant particles interacting with a wave packet (in $\beta < 1$ plasma), an ion-cyclotron resonance occurs. It results in damping of low-k harmonics and growth (instability) of high-k harmonics, which interact with the tail of a particle distribution function. Thus, small-scale bursts may be generated in this regime.

A more detailed investigation of obliquely propagating waves will be presented in future publications.

[2] A. Rogister, Phys. Fluids **14**, 2733 (1971).

[3] E. Mjølhus and J. Wyller, J. Plasma Phys. **40**, 299 (1988).

[4] S. R. Spangler, Phys. Fluids B **2**, 407 (1989).

[5] J. V. Hollweg, Phys. Rev. Lett. **27**, 1349 (1971).

[6] M. A. Lee and H. J. Völk, Astrophys. Space Sci. **24**, 31 (1973).

[7] V. L. Galinsky, A. V. Khrabrov, and V. I. Shevchenko, Plan. Space Sci. **8**, 1069 (1990).

[8] I. I. Shevchenko, V. L. Galinsky, S. K. Ride, and M. Baine, Geophys. Res. Lett. **22**, 2997 (1995).

[9] C. C. Wu, J. Geophys. Res. **93**, 3969 (1988).

[10] C. C. Wu and T. Hada, J. Geophys. Res. **96**, 3755 (1991).

[11] B. J. Vasquez and P. G. Cargill, J. Geophys. Res. **98**, 1277 (1993).

[12] B. J. Vasquez, J. Geophys. Res. **100**, 1779 (1995).

[13] B. J. Vasquez and J. V. Hollweg, J. Geophys. Res. **101**, 13,527 (1996).

[14] M. V. Medvedev and P. H. Diamond, Phys. Plasmas **3** 863 (1996).

[15] S. Raus and J. A. Tataronis, Phys. Plasmas **2**, 1453 (1995).

[16] G. W. Hammett and F. W. Perkins, Phys. Rev. Lett. **64**, 3019 (1990).

[17] V. L. Galinsky, V. I. Shevchenko, M. V. Medvedev, and P. H. Diamond, submitted to Comments Plasma Phys. (1996).

[18] C. F. Kennel, B. Buti, T. Hada, and R. Pellat, Phys. Fluids **30**, 1949 (1988).

[19] S. R. Spangler and B. B. Plapp, Phys. Fluids B **4**, 3356 (1992).

[20] B. T. Tsurutani, C. M. Ho, E. J. Smith, M. Neugebauer,B. E. Goldstein, J. S. Mok, J. K. Arballo, A. Balogh, D. J. Southwood and W. C. Feldman, Geophys. Res. Lett. **21**, 2267 (1994).

[21] E. J. Smith, A. Balogh, M. Neugebauer, and D. J. McComas, Geophys. Res. Lett. **22**, 3381 (1995).

[22] C. M. Ho, B. T. Tsurutani, B. E. Goldstein, J. L. Phillips, and A. Balogh, Geophys. Res. Lett. **22**, 3409 (1995).

[23] R. P. Lepping and K. W. Behannon, J. Geophys. Res. bf 91, 8725 (1986).

[24] B. T. Tsurutani, C. M. Ho, J. K. Arballo, E. J. Smith, B. E. Goldstein, M. Neugebauer, A. Balogh, and W. C. Feldman, J. Geophys. Res. **101**, 11027 (1996).

[25] M. A. Malkov, C. F. Kennel, C. C. Wu, R. Pellat, V. D. Shapiro, Phys. Fluids B **3**, 1407 (1991).

[26] M. A. Malkov, R. Z. Sagdeev, V. D. Shapiro, Physics Letters A **151**, 505 (1990).

[27] D. J. Kaup and A. C. Newell, J. Math. Phys. **19**, 798 (1978).

[28] J. Wyller, T. Flå, and E. Mjølhus, Physica D **39**, 405 (1989).

[29] E. Mjølhus, Physica Scripta **40**, 227 (1989).

[30] S. P. Dawson and C. F. Fontan, Phys. Fluids **31**, 83 (1988).

[31] T. Flå, E. Mjølhus, J. Wyller, Phys. Scr. **40**, 219 (1989).

[32] E. Mjølhus and J. Wyller, Physica Scripta **33**, 442 (1986).

[1] R. H. Cohen and R. M. Kulsrud, Phys. Fluids **17**, 2215 (1974).

DNLS, linear polarization
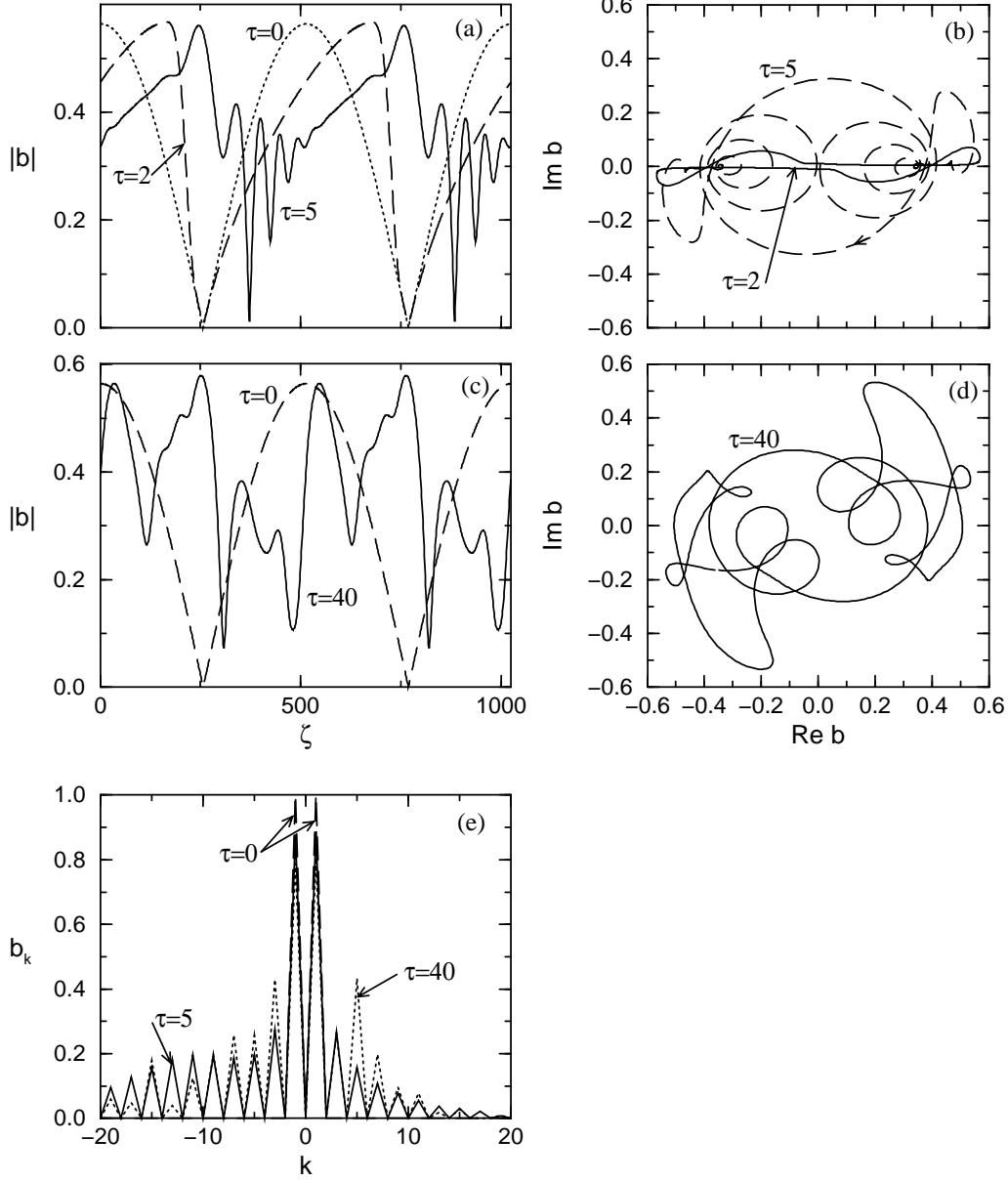
FIG. 1.   Wave evolution from the DNLS with $\beta = 0, M_1 = 1, M_2 = 0$ for *linearly* polarized, sinusoidal wave initial condition. (a) and (c) - wave profiles, (b) and (d) - phase diagrams (hodographs), (e) - harmonic spectra at $\tau = 0, 5, 40$. At $\tau = 0$ only $k = 1, -1$ harmonics are excited. Note an irregular wave structure at late times (i.e. $\tau = 40$).

DNLS, circular polarization
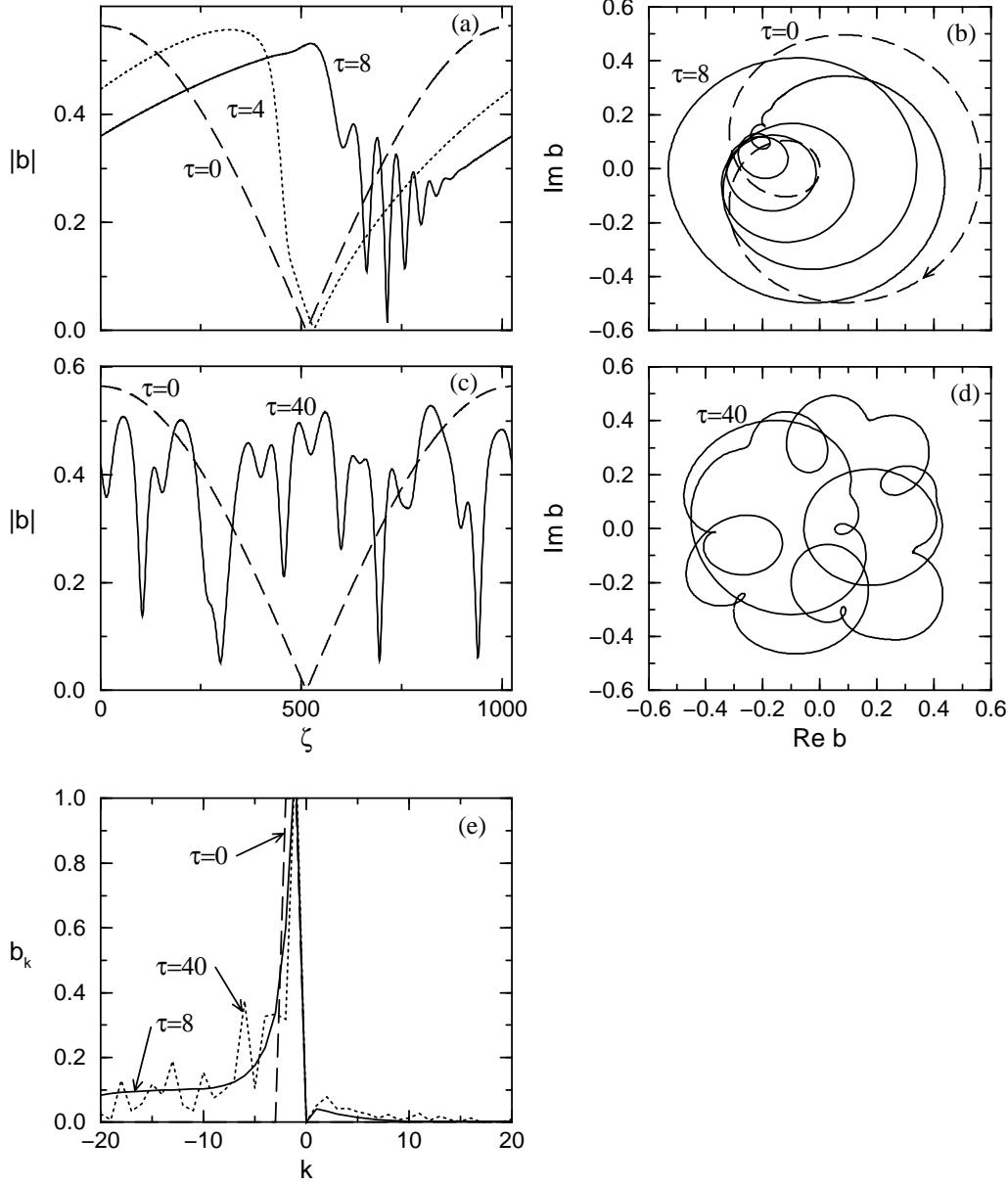
FIG. 2. Wave evolution from the DNLS with $\beta = 0$ for *circularly* polarized, sinusoidally amplitude modulated initial condition. (a) and (c) - wave profiles, (b) and (d) - phase diagrams (hodographs), (e) - harmonic spectra at $\tau = 0, 8, 40$. At $\tau = 0$ only $k = -1, -2$ harmonics are excited. Note the irregular wave structure at late times $\tau = 40$.
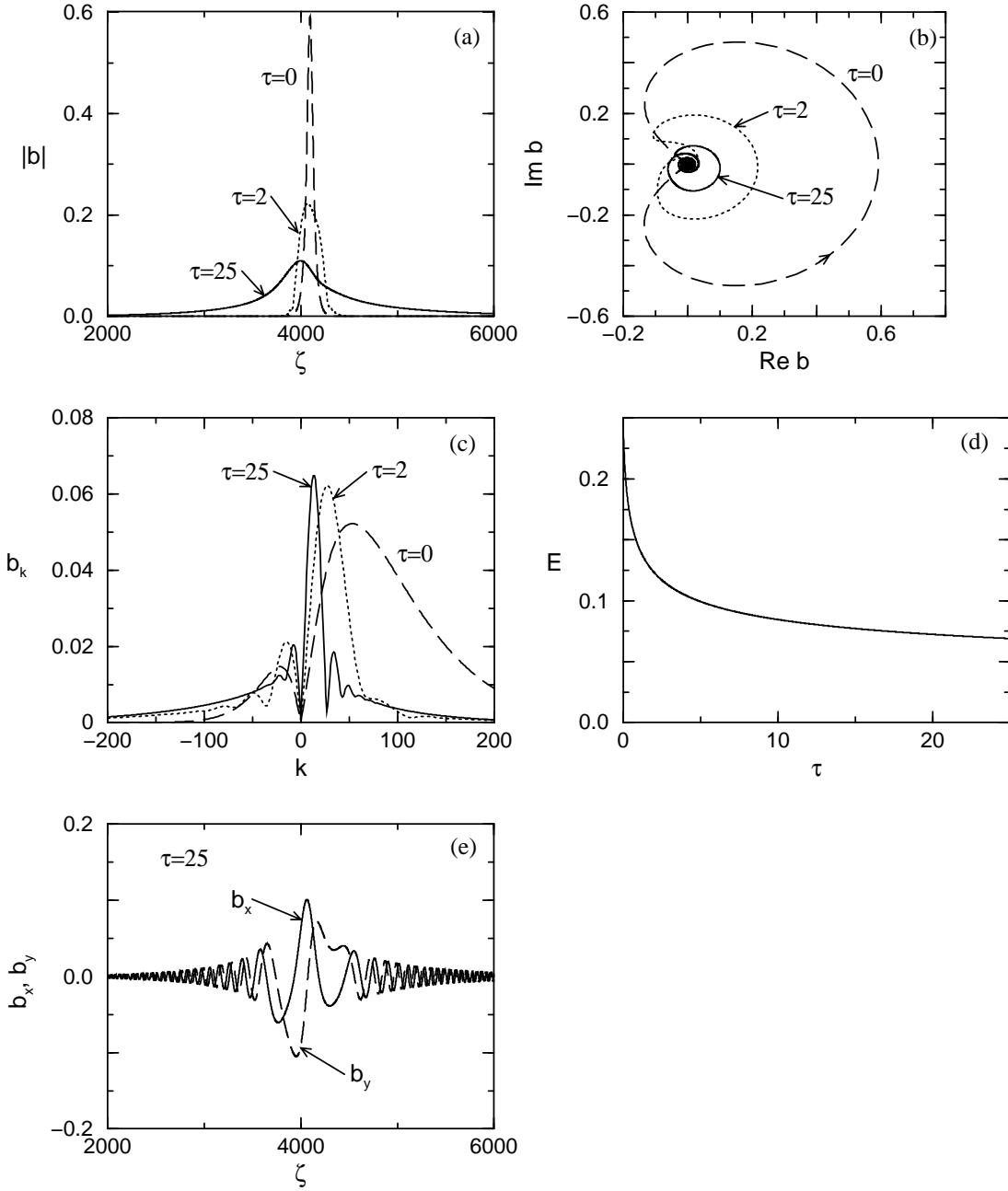
FIG. 3. Evolution for a parallel propagating, *soliton* initial condition for the KNLS with Landau damping for $\beta = 1$, $M_1 = 1.5$, $M_2 = -1.63$ at $\tau = 0, 2, 25$. (a) - wave packet spatial profile, (b) - hodographs, (c) - harmonic spectra, (d) - temporal evolution of wave energy, (e) - profiles of the wave magnetic fields b_x and b_y at $\tau = 25$.

Landau, linear polarization
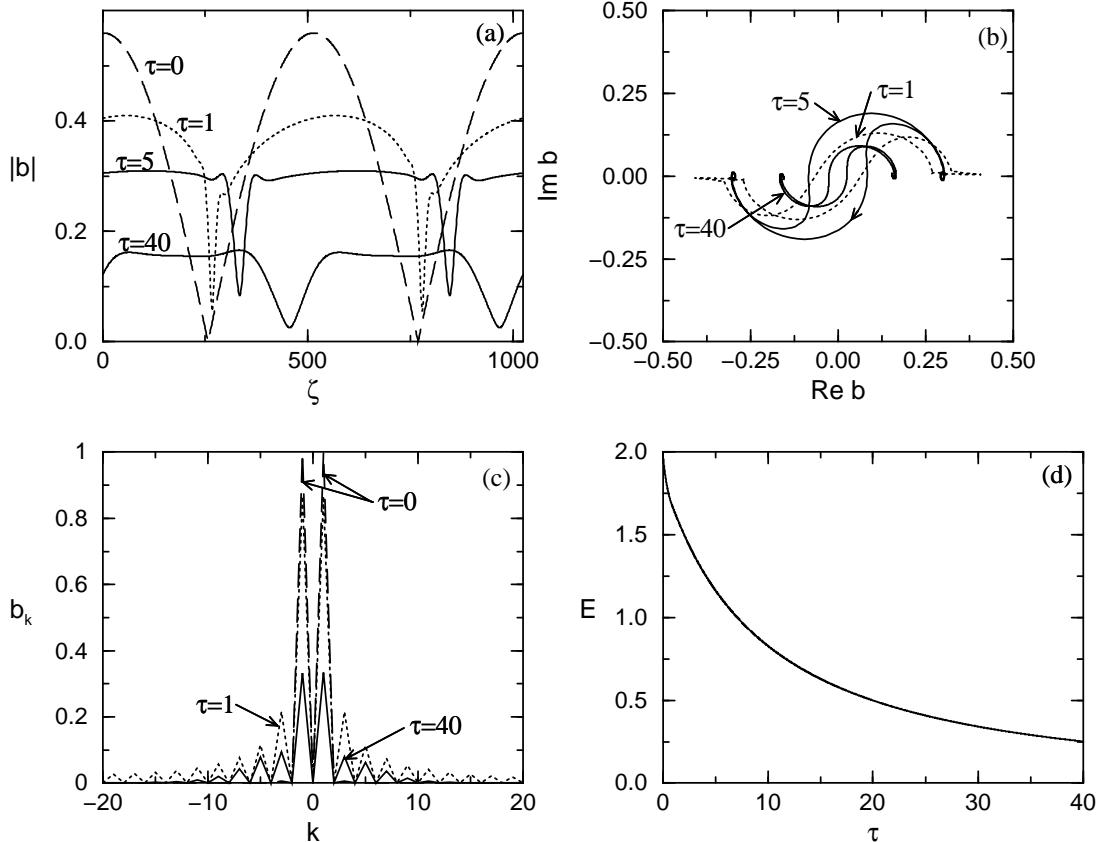
FIG. 4. Wave evolution from the KNLS with Landau damping for $\beta = 1$, $M_1 = 1.5$, $M_2 = -1.63$ for a parallel propagating, *linearly* polarized sinusoidal wave initial condition. (a) - wave profiles, (b) - hodographs, (c) - harmonic spectra, (d) - temporal evolution of wave energy. At $\tau = 0$ only $k = 1, -1$ harmonics are excited. Note the formation of localized, quasi-stationary waveforms (*dissipative structures*) with a characteristic S-shaped phase diagram and narrow harmonic spectrum.

Landau, linear polarization
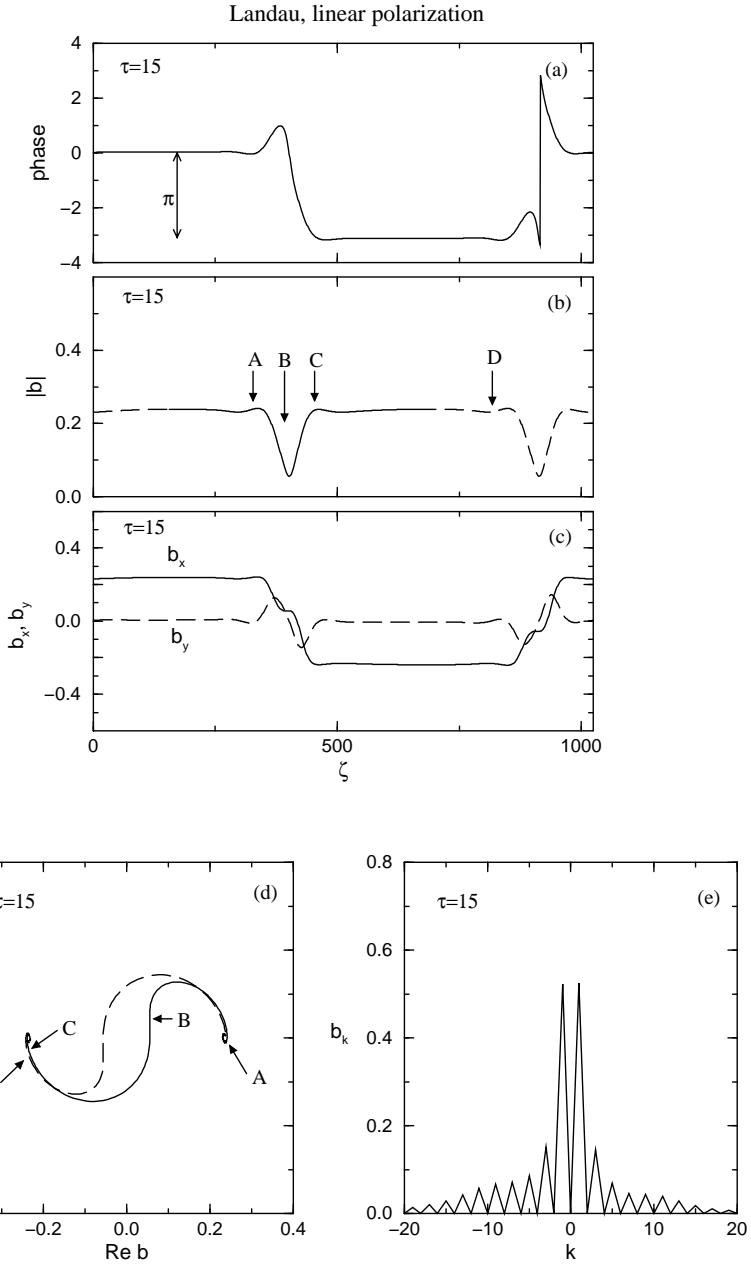
FIG. 5. Detailed snapshot of a *dissipative structure* (or a KNLS rotational/directional discontinuity) at $\tau = 15$ in $\beta = 1$ plasma. (a) - phase profile, (b) - wave amplitude profile, (c) - profiles of the wave fields b_x, b_y (note narrow spatial localization of the discontinuity), (d) - hodograph (note a characteristic *S-shape*), (e) -harmonic spectrum.

19

Landau, circular polarization
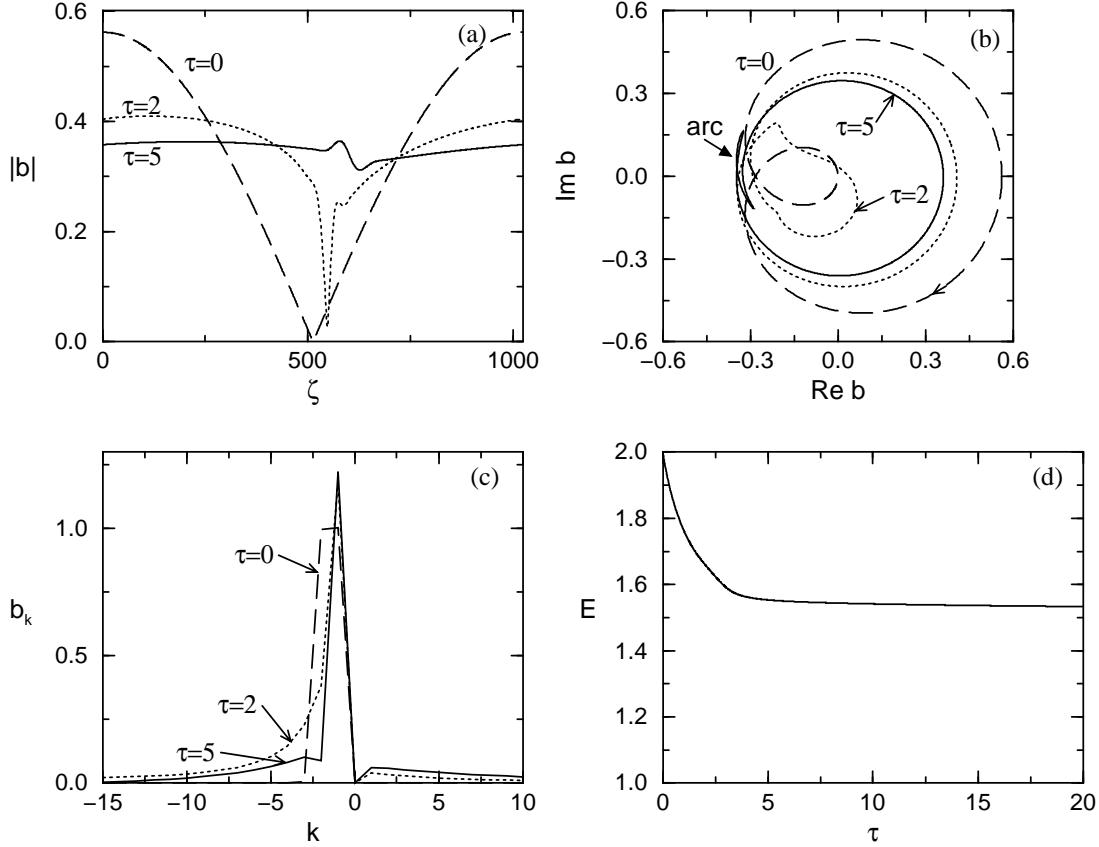
FIG. 6. Wave evolution for the KNLS with Landau damping for $\beta = 1$, $M_1 = 1.5$, $M_2 = -1.63$ for a parallel propagating, *circularly* polarized sinusoidal wave initial condition. (a) - wave profiles, (b) - hodographs, (c) - harmonic spectra, (d) - temporal evolution of wave energy. At $\tau = 0$ only $k = -1, -2$ harmonics are excited. Note the formation of an intermittent, arc-polarized discontinuity at $\tau = 5$, which disappears quickly due to Landau damping. Only $k = -1$ circularly polarized harmonic survives and experience no steepening or damping.

Landau, elliptical polarization
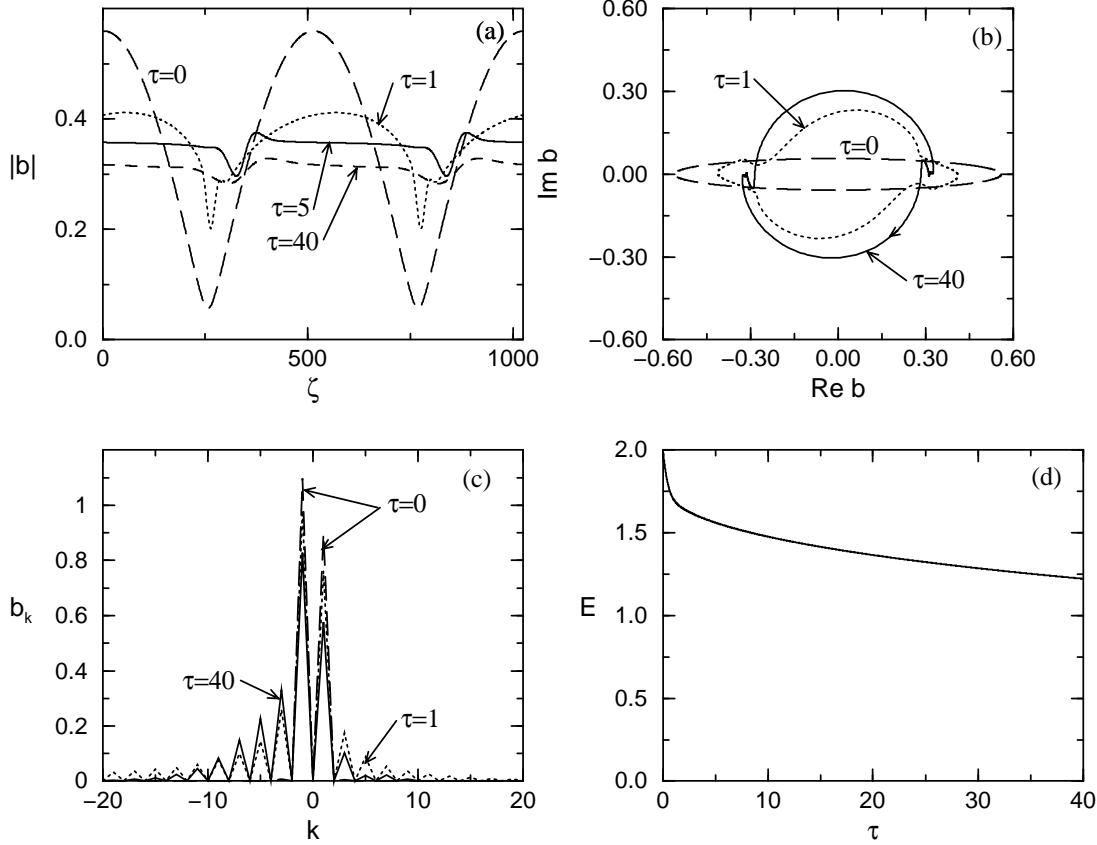
FIG. 7. Wave evolution for the KNLS with Landau damping for $\beta = 1$, $M_1 = 1.5$, $M_2 = -1.63$ for a parallel propagating, *elliptically* polarized sinusoidal wave initial condition. (a) - wave profiles, (b) - hodographs, (c) - harmonic spectra, (d) - temporal evolution of wave energy. At $\tau = 0$ only $k = 1, -1$ harmonics are excited and $b_1 = 0.9, b_{-1} = 1.1$. Note the formation of rotational discontinuities (phase change equal to π radians) with weak wave amplitude variation across. Note also the smaller energy dissipation rate than for a linear polarization.
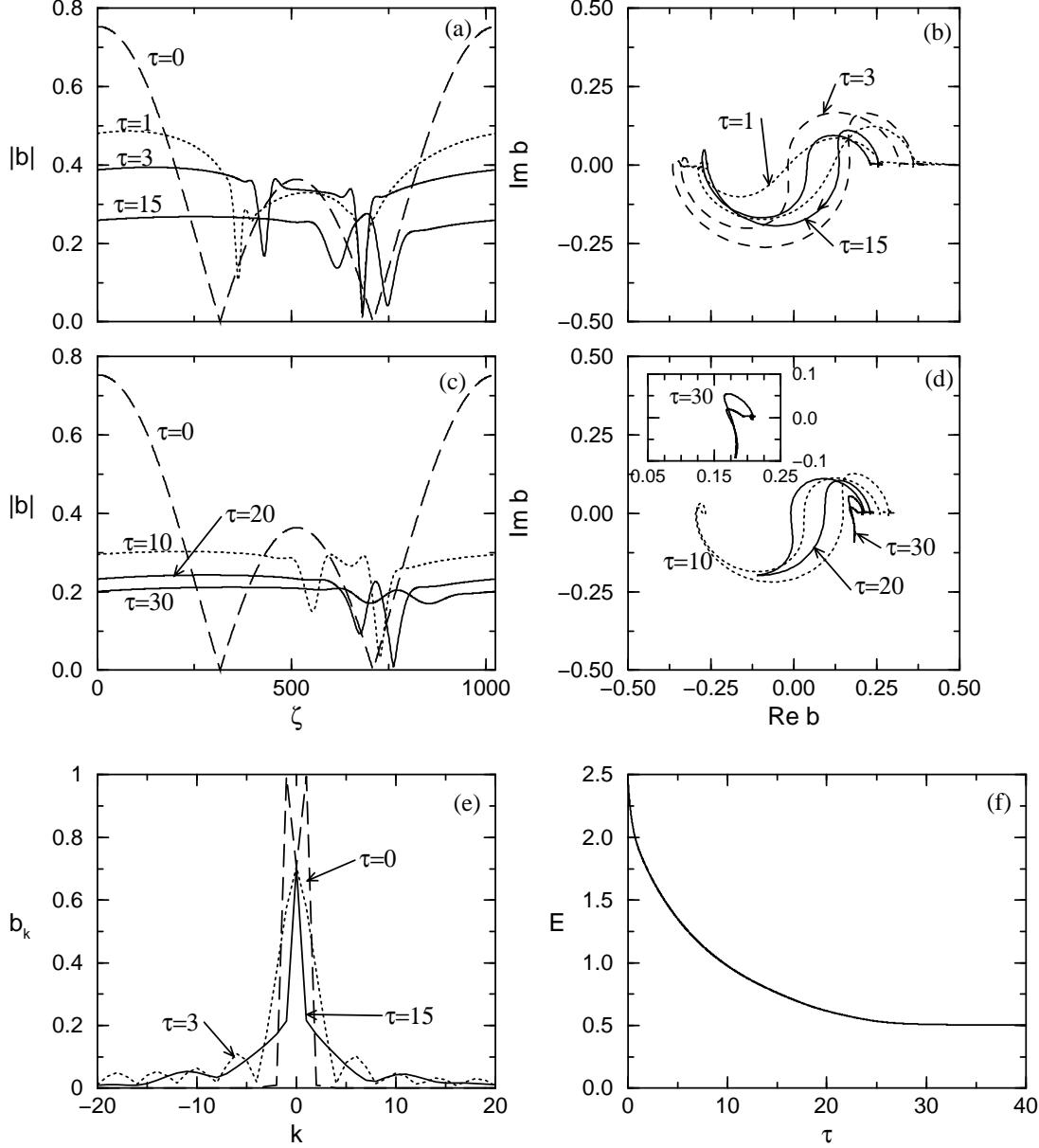
FIG. 8. Wave evolution for the KNLS with Landau damping for $\beta = 1$, $M_1 = 1.5$, $M_2 = -1.63$ for an *obliquely* propagating ($\Theta = 45°$), *linearly* polarized, *longitudinal*, sinusoidal wave initial condition. (a) and (c) - wave profiles, (b) and (d) - hodographs, (e) - harmonic spectra, (f) - temporal evolution of wave energy. At $\tau = 0$ only $k = 1, -1$ harmonics are excited. Note the formation of two KNLS directional discontinuities which interact and annihilate with each other (at $\tau \simeq 20$) to yield a weakly dissipative, small amplitude residual wave structure.

Landau, circular polarization, oblique propagation
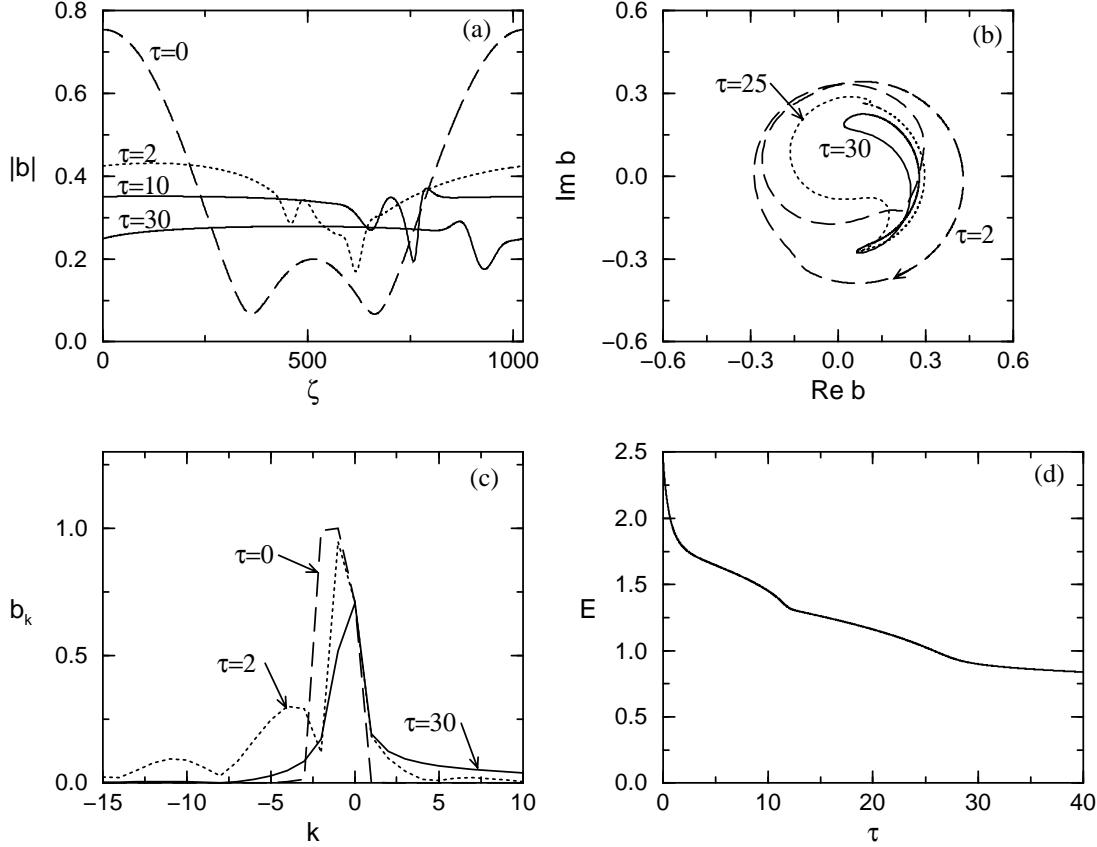
FIG. 9. Wave evolution for the KNLS with Landau damping for $\beta = 1$, $M_1 = 1.5$, $M_2 = -1.63$ for an *obliquely* propagating, *circularly* polarized, *longitudinal*, sinusoidal wave initial condition. (a) - wave profiles, (b) - hodographs, (c) - harmonic spectra, (d) - temporal evolution of wave energy. At $\tau = 0$ only $k = -1, -2$ harmonics are excited. Note the formation of a stationary *arc-polarized rotational discontinuity* at approximately $\tau = 25$.

Landau, circular polarization, oblique propagation
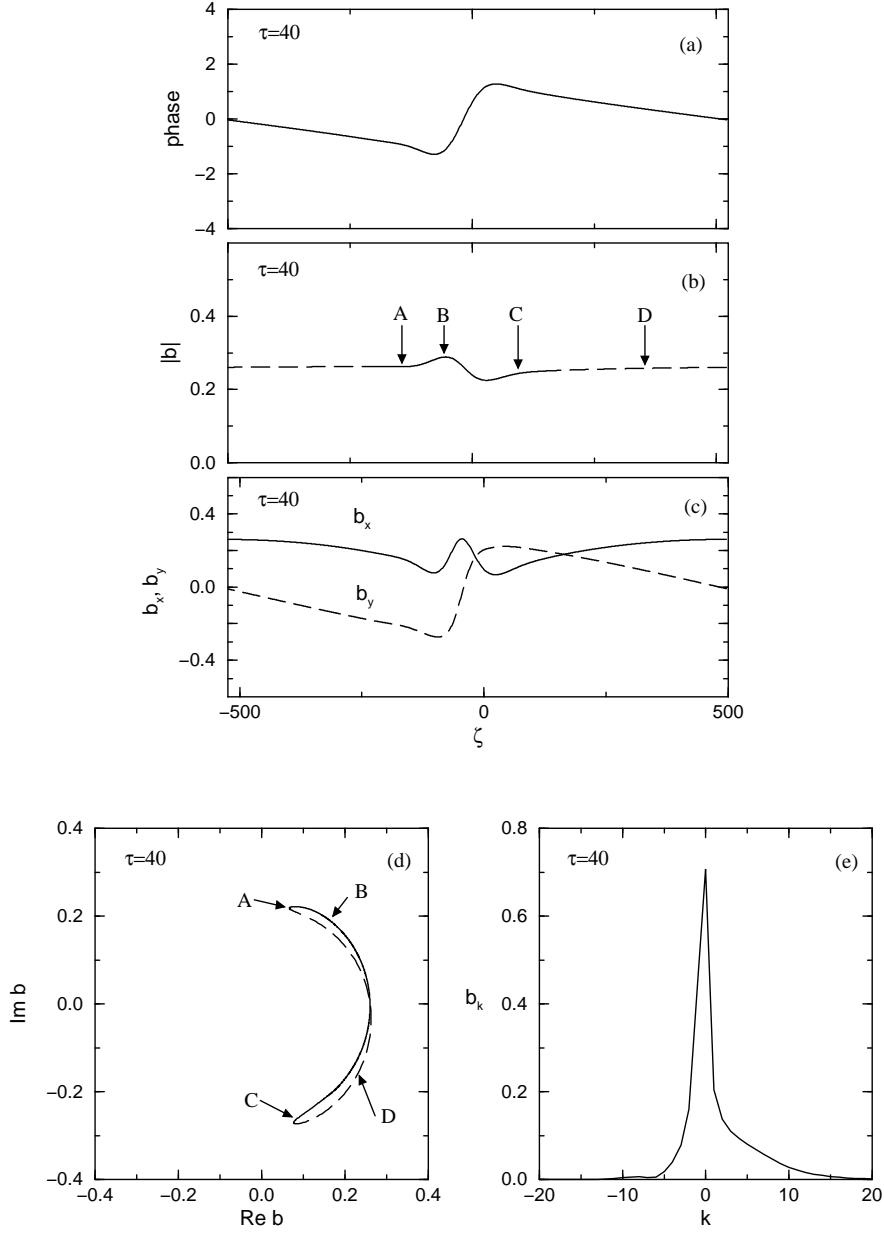
FIG. 10. Detailed snapshot of an *arc-polarized rotational discontinuity* at $\tau = 40$ for $\beta = 1$ plasma. (a) - phase profile, (b) - wave amplitude profile, (c) - profiles of the wave fields b_x, b_y (note the narrow spatial localization of the discontinuity and the negligible wave amplitude modulation), (d) - hodograph (note a characteristic *arc-shape*), (e) -harmonic spectrum.

Landau, linear polarization, oblique propagation, transverse wave
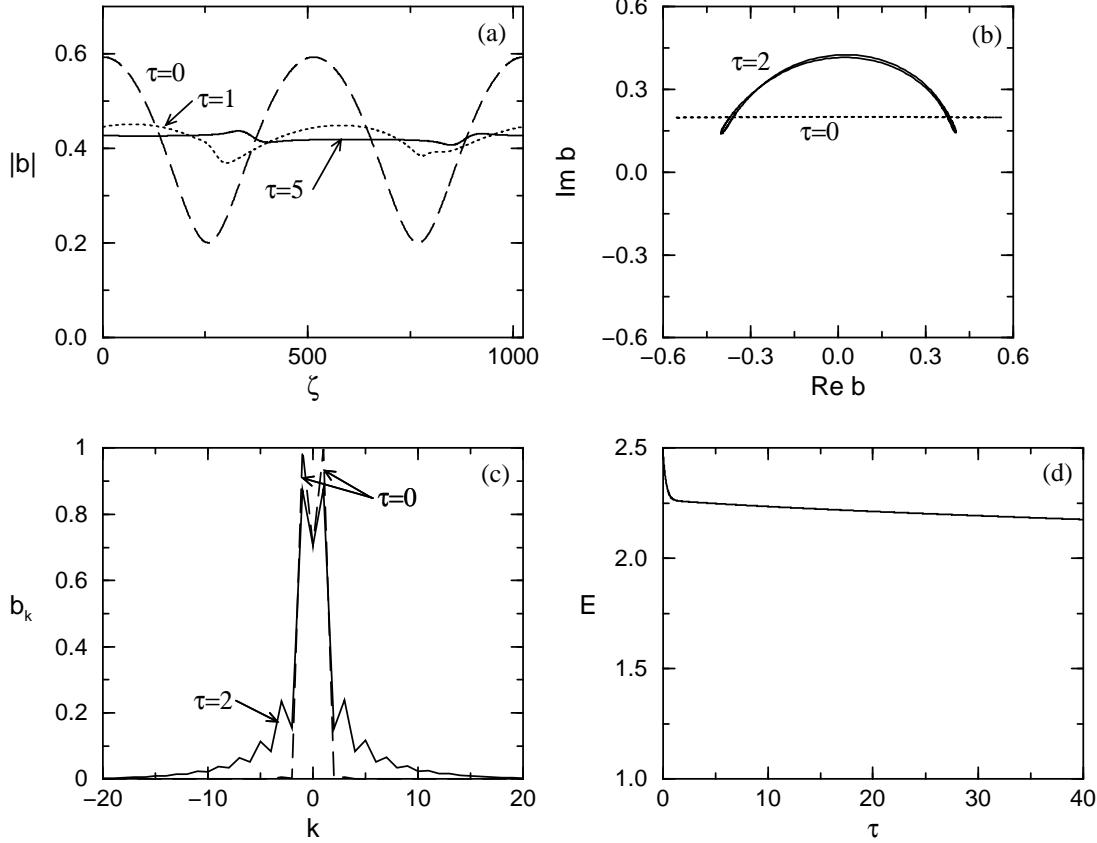
FIG. 11. Wave evolution for the KNLS with Landau damping for $\beta = 1$, $M_1 = 1.5$, $M_2 = -1.63$ for an *obliquely* propagating, *trasversal*, sinusoidal wave initial condition. (a) - wave profiles, (b) - hodographs, (c) - harmonic spectra, (d) - temporal evolution of wave energy. At $\tau = 0$ only $k = 1, -1$ harmonics are excited. Note the formation of a stationary *arc-polarized rotational discontinuity* at approximately $\tau = 2$.
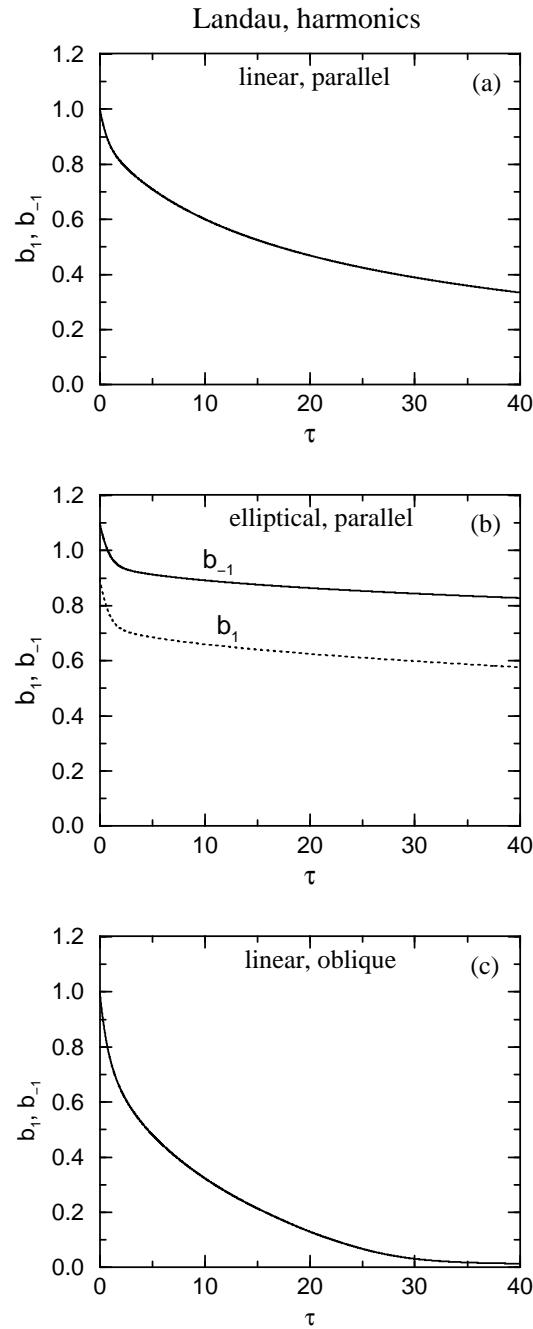
FIG. 12. Temporal evolution of two initially excited harmonics for the KNLS for $\beta = 1$ for a (a) parallel propagating, linearly polarized wave (b_{-1} and b_1 harmonics overlaid), (b) parallel propagating, elliptically polarized wave, and (c) obliquely propagating ($\Theta = 45°$), linearly polarized wave.

Collisional, soliton
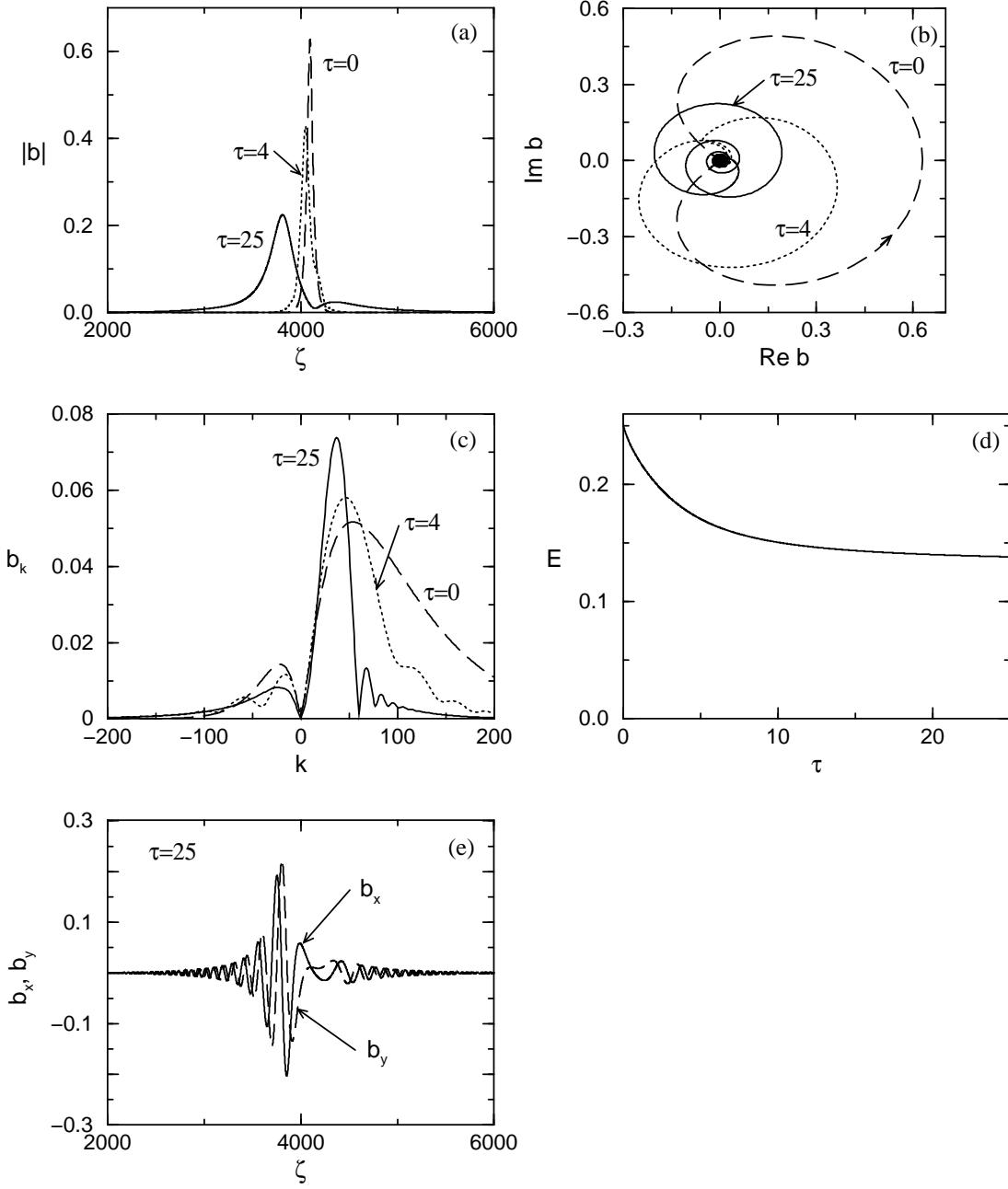
FIG. 13. Evolution for a parallel propagating, *soliton* initial condition for the KNLS with collisional damping for $\beta = 0.99$ and $\kappa = 100$ ($\kappa \simeq k_{\text{typical}}$ corresponds to the strongest damping) at $\tau = 0, 4, 25$. (a) - wave packet spatial profile, (b) - hodographs, (c) - harmonic spectra, (d) - temporal evolution of wave energy, (e) - profiles of the wave magnetic fields b_x and b_y at $\tau = 25$.
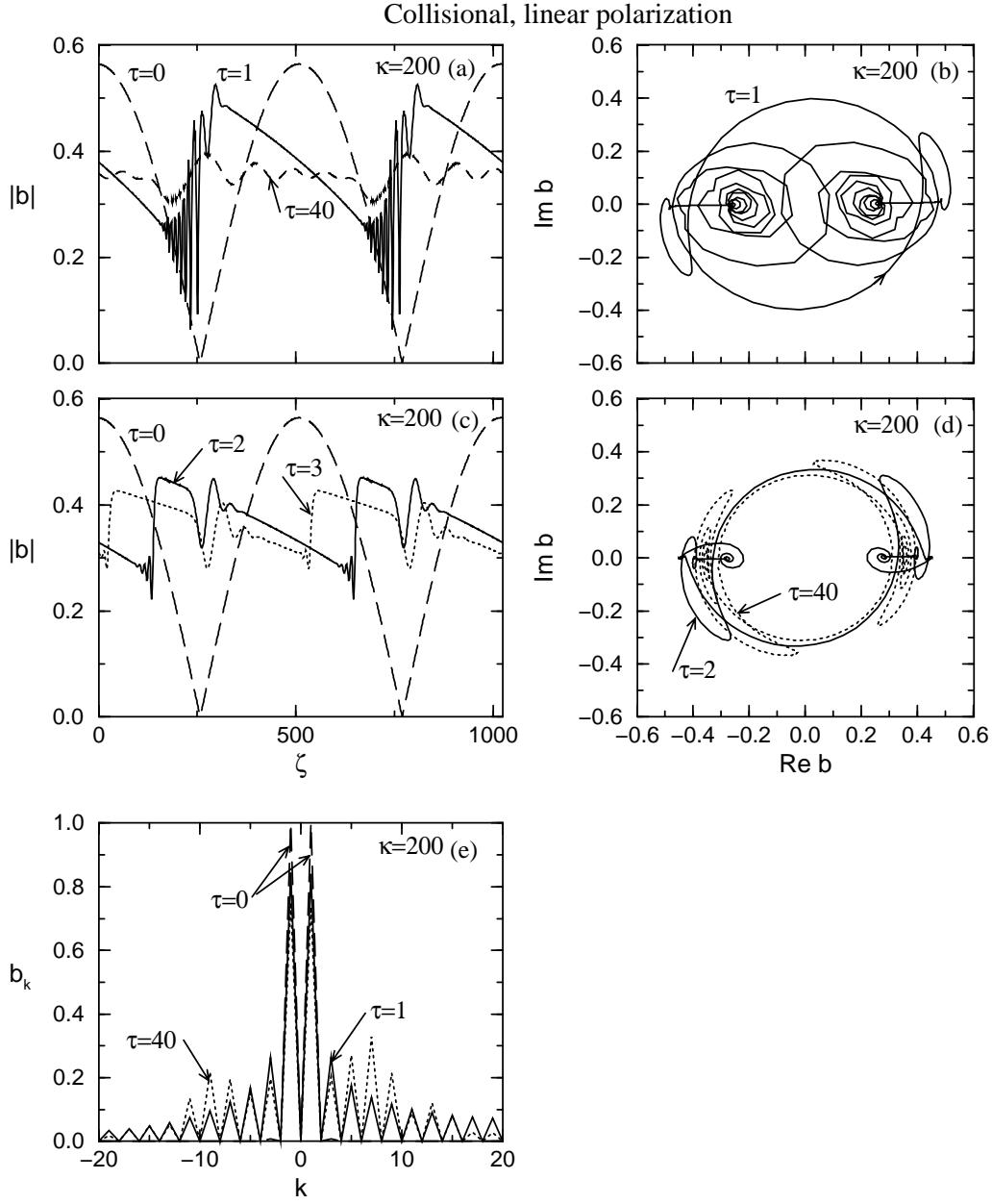
FIG. 14. Wave evolution for the KNLS with collisional damping with $\beta = 0.99$ and $\kappa = 200$ (weakly collisional regime) for parallel propagating, *linearly* polarized sinusoidal wave initial condition. (a) and (c) - wave profiles, (b) and (d) - hodographs, (e) - harmonic spectra. At $\tau = 0$ only $k = 1, -1$ harmonics are excited. Note the formation of propagating shock waves (sharp fronts) and rotational discontinuities (wider wave-like forms). The noisy parasitic oscillations generated at earlier times ($\tau = 1$) are possibly due to modulation instability, which is stronger for smaller scale modulations.
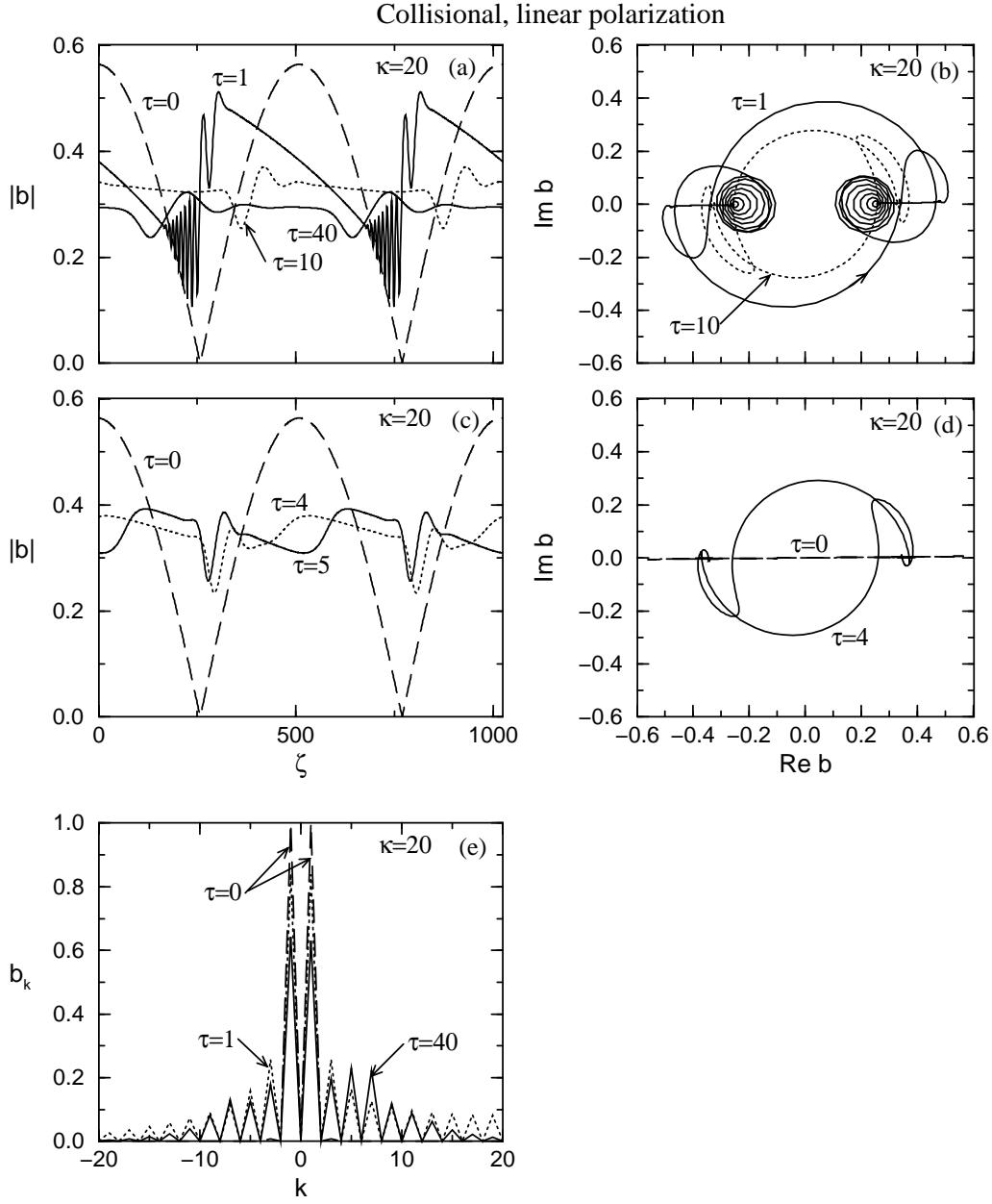
FIG. 15. Wave evolution for the KNLS with collisional damping with $\beta = 0.99$ and $\kappa = 20$ (intermediate collisional regime) for parallel propagating, *linearly* polarized sinusoidal wave initial condition. (a) and (c) - wave profiles, (b) and (d) - hodographs, (e) - harmonic spectra. At $\tau = 0$ only $k = 1, -1$ harmonics are excited. The width of a shock wave is wider (as controlled by collisions), however the width of the rotational discontinuity is the same, i.e. it is controlled by the dispersion parameter, alone.

Collisional, linear polarization
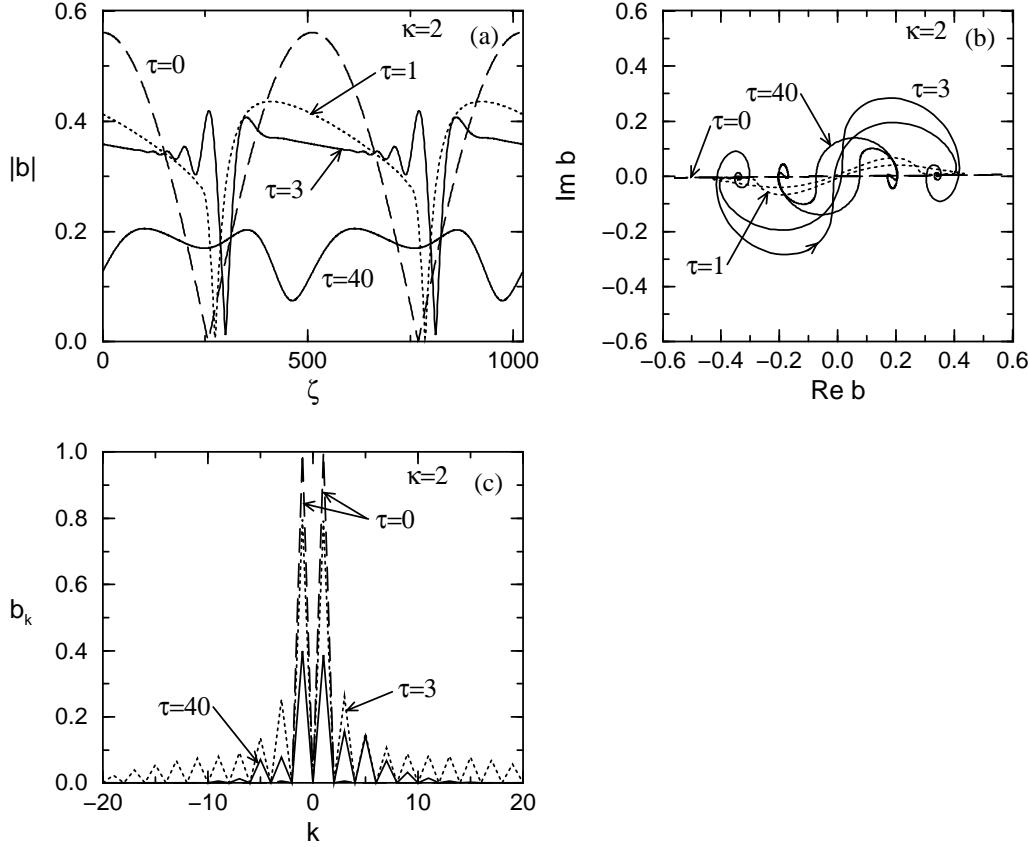
FIG. 16. Wave evolution for the KNLS with collisional damping with $\beta = 0.99$ and $\kappa = 2$ (strongly collisional regime) for a parallel propagating, *linearly* polarized sinusoidal wave initial condition. (a) and (c) - wave profiles, (b) and (d) - hodographs, (e) - harmonic spectra. At $\tau = 0$ only $k = 1, -1$ harmonics are excited. Note the remarkable similarity to the case of Landau damping.

Collisional, linear polarization
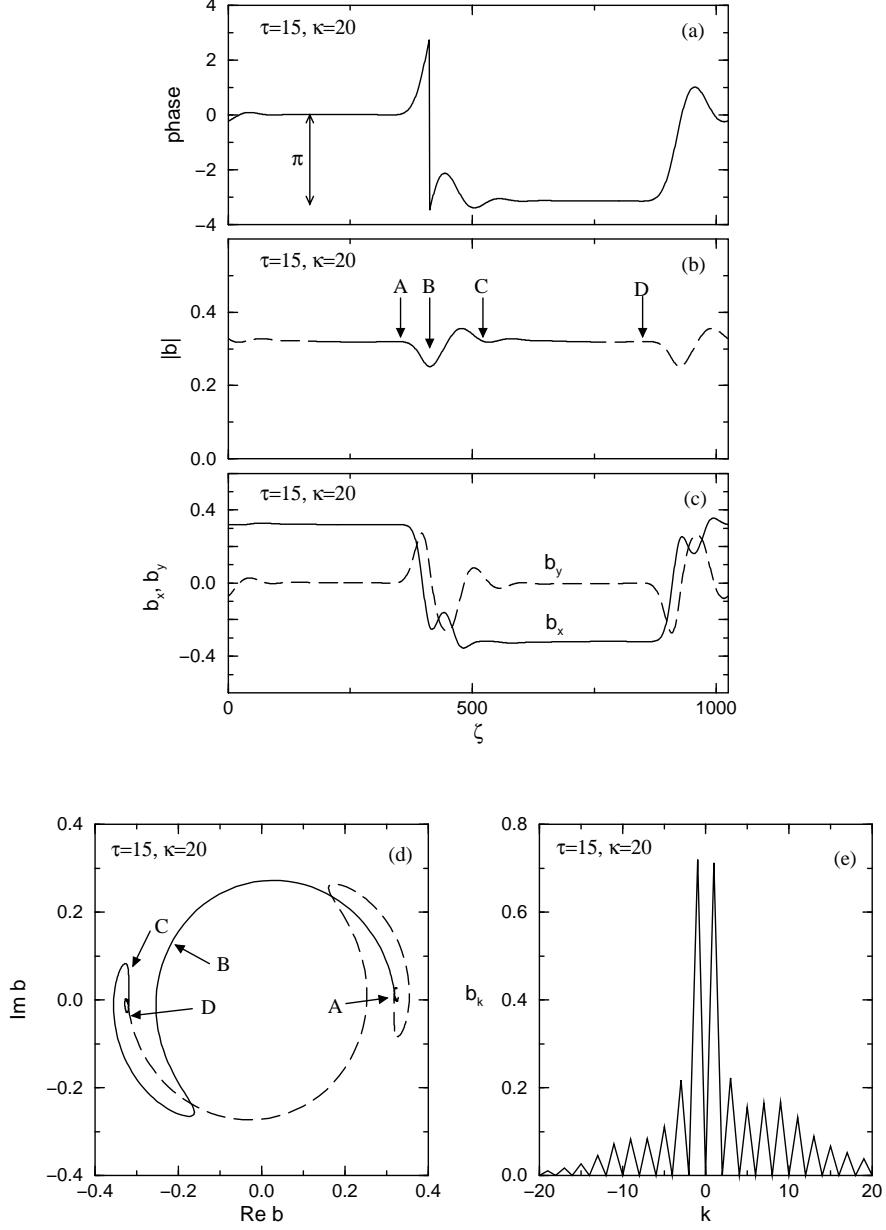
FIG. 17. Detailed snapshot of a *rotational discontinuity* for an intermediate collisional regime ($\kappa = 20$) at $\tau = 15$ in $\beta = 0.99$ plasma. (a) - phase profile, (b) - wave amplitude profile, (c) - profiles of the wave fields b_x, b_y (note narrow spatial localization of the discontinuity), (d) - hodograph (note a typical *S-shape*), (e) -harmonic spectrum.

Collisional, linear polarization
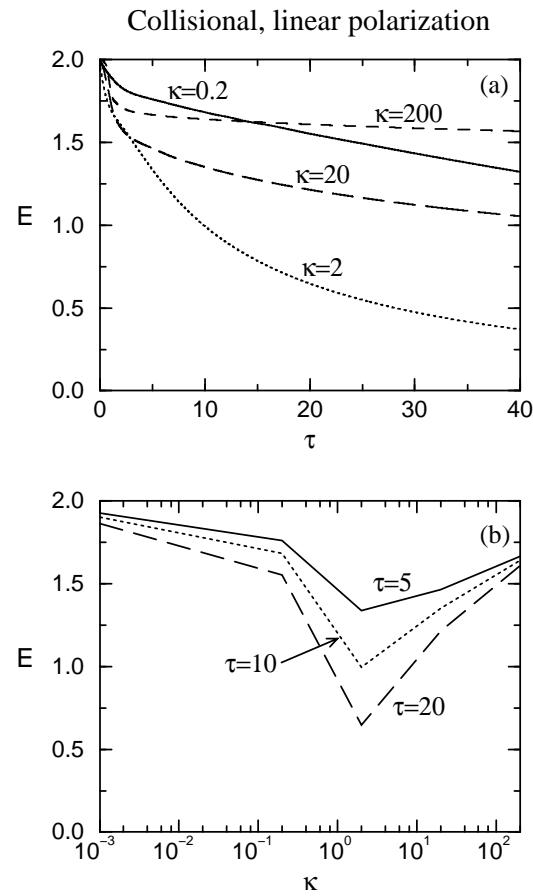
FIG. 18. Wave energy evolution: (a) - temporal evolution of wave energy im different collisional regimes. (b) - wave energy content at times $\tau = 5, 10, 20$ as a function of plasma collisionality, κ.

Collisional, linear polarization
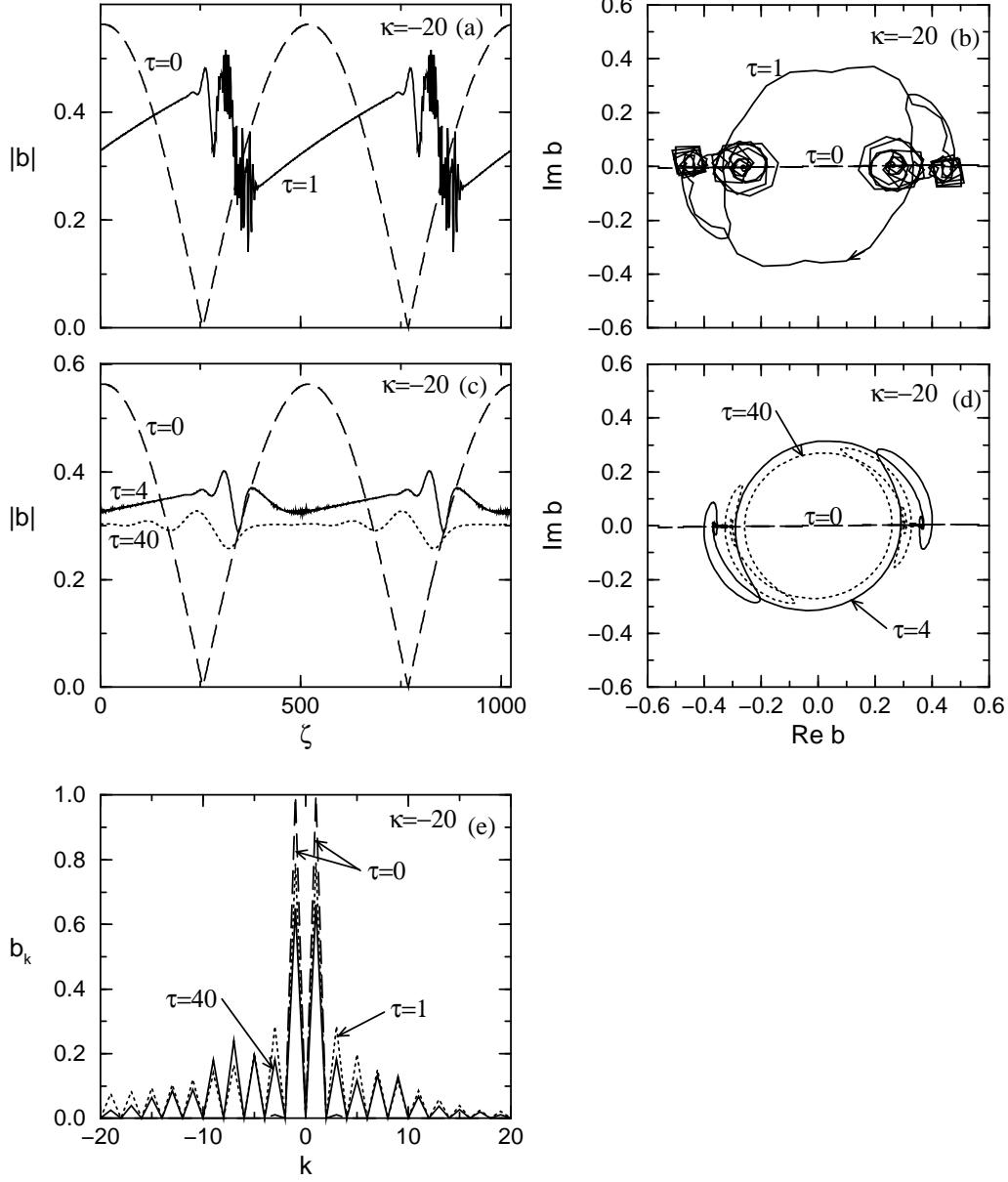
FIG. 19. Wave evolution for the KNLS with collisional damping for $\beta = 1.01$ and $\kappa = -20$ (intermediate collisional regime) for a parallel propagating, *linearly* polarized sinusoidal wave initial condition. (a) and (c) - wave profiles, (b) and (d) - hodographs, (e) - harmonic spectra. At $\tau = 0$ only $k = 1, -1$ harmonics are excited. Wavefront steepening occurs at the front face, thus it is controlled by the sign of κ (the nonlinear dispersion effect).

Collisional, circular polarization
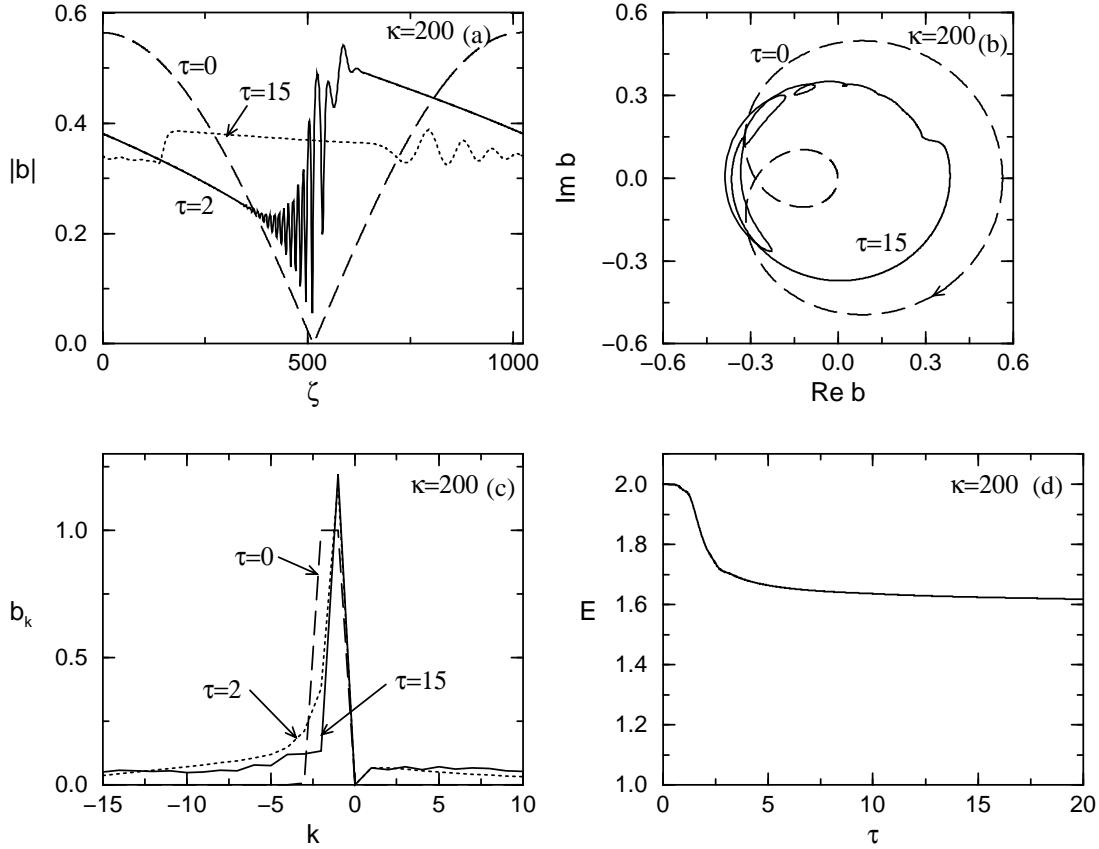
FIG. 20. Wave evolution for the KNLS with collisional damping for $\beta = 0.99$ and $\kappa = 200$ (weakly collisional regime) for a parallel propagating, *circularly* polarized sinusoidal wave initial condition. (a) - wave profiles, (b) - hodographs, (c) - harmonic spectra, (d) - temporal evolution of wave energy. At $\tau = 0$ only $k = -1, -2$ harmonics are excited. A sharp front (shock) still forms, but phase irregularities form instead of a rotational discontinuity.

Finite Larmor, linear polarization
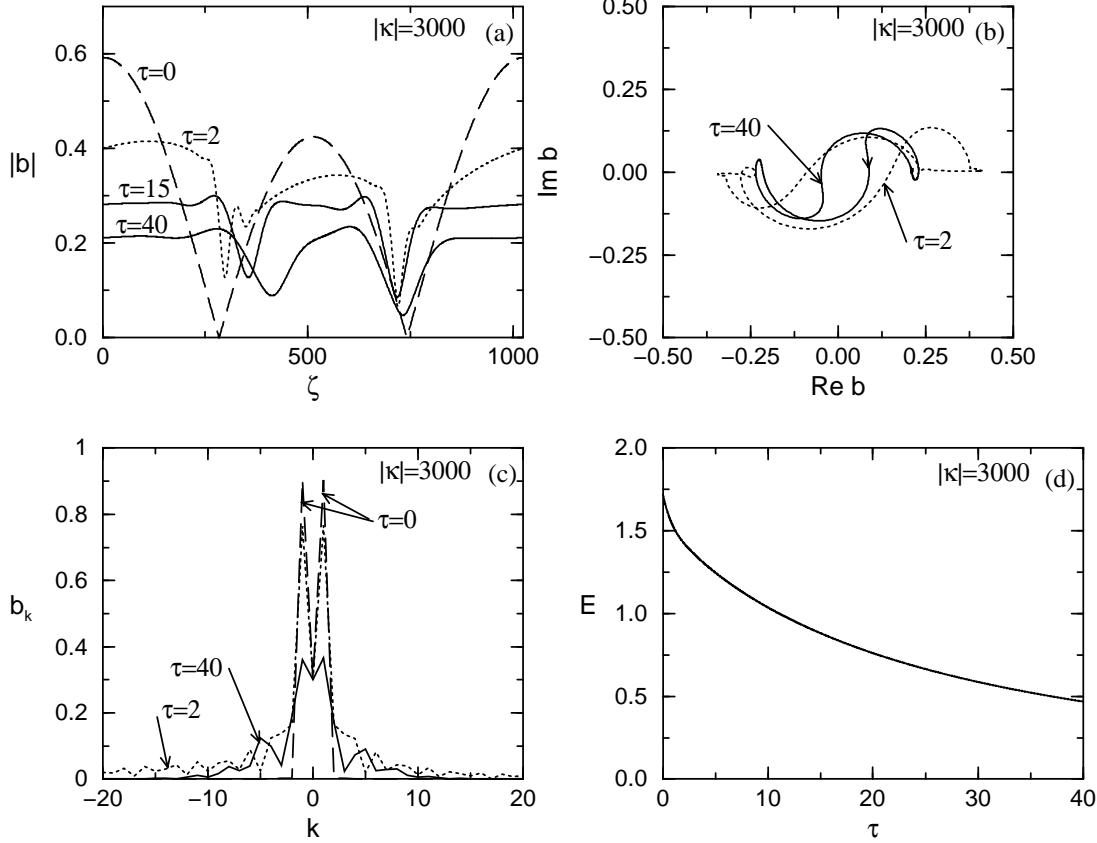
FIG. 21. Wave evolution for the KNLS with Landau damping and gyro-kinetic effects for $\kappa^2 < 0$, $|\kappa| = 3000$ (typical $k\rho_i \simeq 0.002$), and $\beta = 0.9$ for an *obliquely* propagating ($\Theta = 30°$), *linearly* polarized sinusoidal wave initial condition. (a) - wave profiles, (b) - hodographs, (c) - harmonic spectra, (d) - temporal evolution of wave energy. At $\tau = 0$ only $k = 1, -1$ harmonics are excited. Observe that S-type rotational/directional discontinuities form.

Finite Larmor, circular polarization
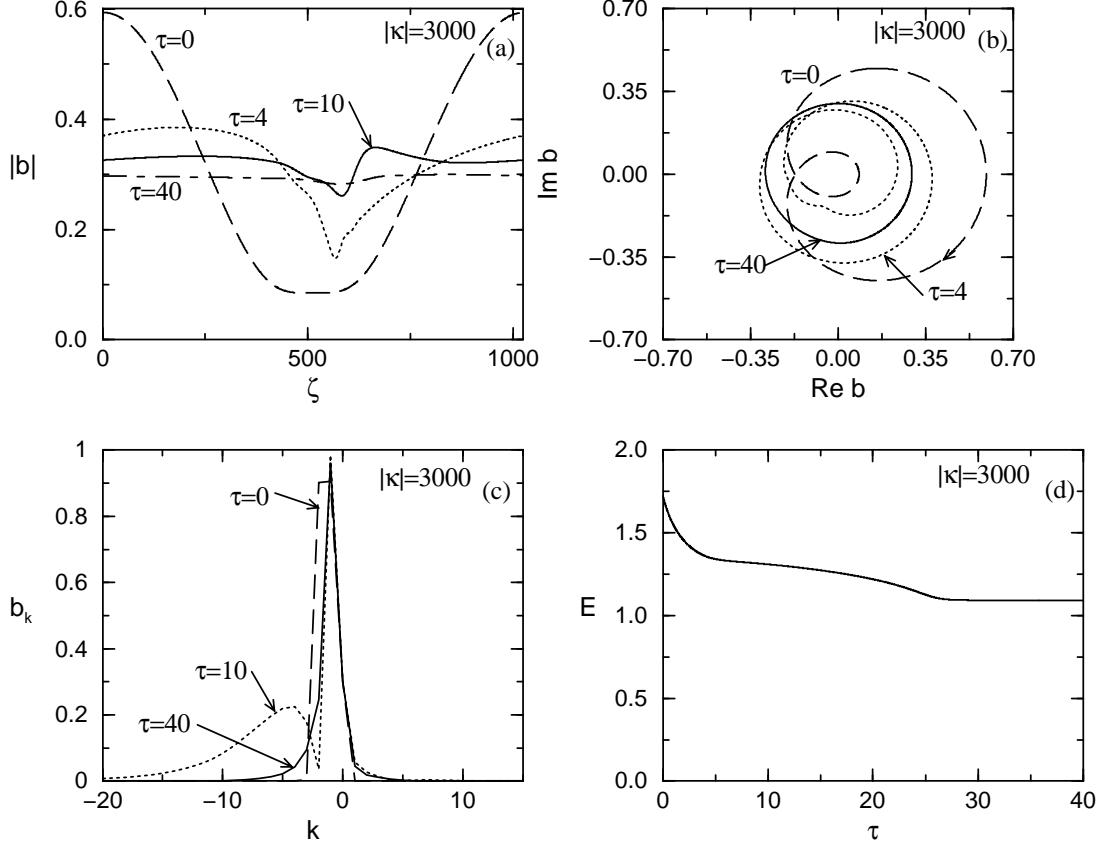
FIG. 22. Wave evolution for the KNLS with Landau damping and gyro-kinetic effects for $\kappa^2 < 0$, $|\kappa| = 3000$ (typical $k\rho_i \simeq 0.002$), and $\beta = 0.9$ for an *obliquely* propagating ($\Theta = 30°$), *circularly* polarized sinusoidal wave initial condition. (a) - wave profiles, (b) - hodographs, (c) - harmonic spectra, (d) - temporal evolution of wave energy. At $\tau = 0$ only $k = -1, -2$ harmonics are excited. Note that arc-type rotational discontinuities do not form.

Finite Larmor, linear polarization
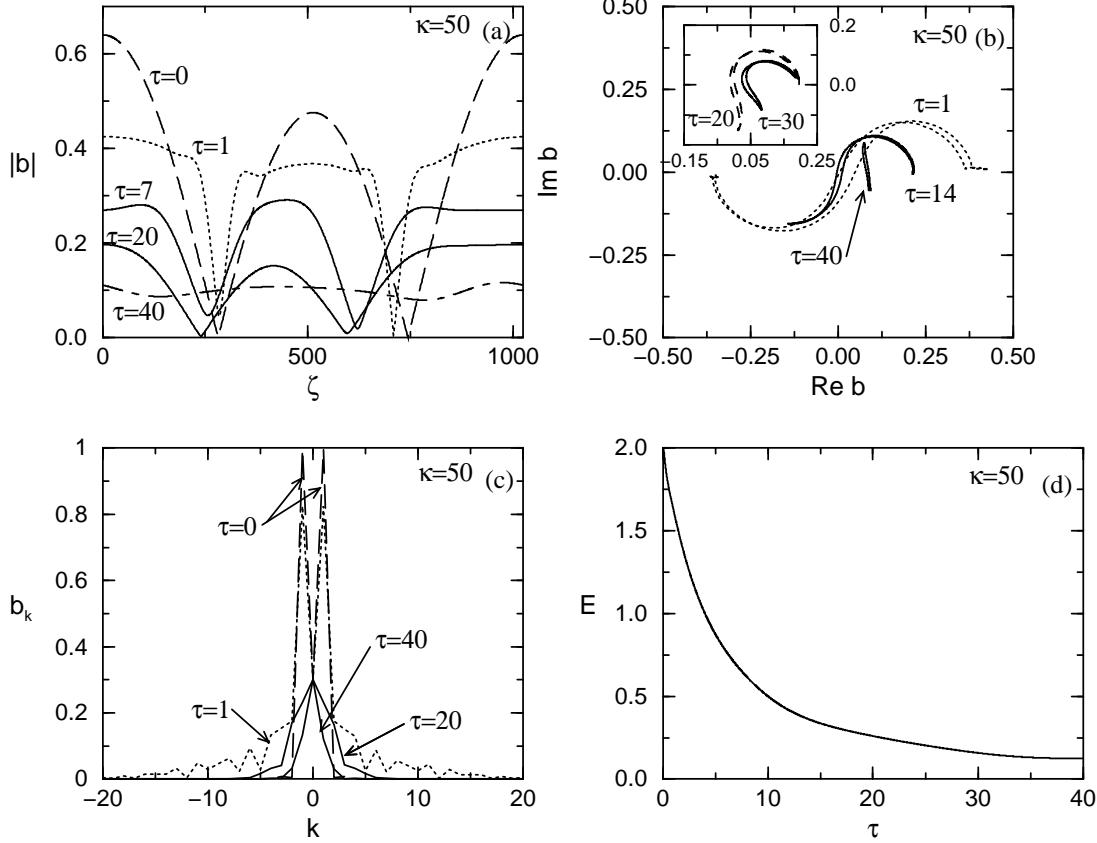
FIG. 23. Wave evolution for the KNLS with Landau damping and gyro-kinetic effects for $\kappa^2 > 0$, $|\kappa| = 50$ (large Larmor radius, typical $k\rho_i \simeq 0.1$), and $\beta = 1.3$ for an *obliquely* propagating ($\Theta = 30°$), *linearly* polarized sinusoidal wave initial condition. (a) - wave profiles, (b) - hodographs, (c) - harmonic spectra, (d) - temporal evolution of wave energy. At $\tau = 0$ only $k = 1, -1$ harmonics are excited.

kinetic effect and $\Delta\beta$	propagation direction, Θ	initial wave, $\tau = 0$	intermediate waveform, $\tau \sim 5-10$	steady state waveform, $\tau \geq 40$	energy dissipation (steady state)	remarks
no,	parallel,	linear	radiation of			strong
	$\Theta = 0°$	circular	solitons	irregular	no	DNLS
$\beta \sim 0$	oblique,	linear	at the	structures	dissipation	soliton
	$\Theta \sim 30°$	circular	steep edge			turbulence
Landau	parallel,	linear	*S-polarized DD* & lin.-polarized wave	**S-polarized DD, $\Delta\phi = \pi$**	strong	**dissipative structures**
	$\Theta = 0°$	elliptic	*arc-polarized RD* & lin.-polarized wave	**arc-polarized R.D, $\Delta\phi = \pi$**	weak	intermediate of lin. and circ. waves
		circular	*arc* polarization & circ.-polarized wave	pure circular wave	no (strong: $\tau < 5$)	**single, lowest-k harmonic**
damping,	oblique,	linear, longitud.	*S-polarized* RD/DD's, $\to$ interact/annihilate	small-amplitude background	strong until "annihilation"	background: $\sim$ arc-polarized
		elliptic, longitud.	*arc-polarized RD* & lin.-polarized wave		no (weak: $\tau < 50$)	evolution is slower than for circ. wave
$.5 \leq \beta \leq 1.5$	$\Theta \sim 45°$	linear, transver.	**arc-polarized RD,**	**arc-polarized R.D,**	no	very fast evolution; large wave energy content
		elliptic, transver.	**$\Delta\phi < \pi$**	**$\Delta\phi < \pi$**	no (weak: $\tau < 2$)	
		circular	modulated circular wave		no (weak: $\tau < 30$)	broad spectrum of *arc-* RD
Collisional (diffusive) dissipation, $.95 \leq \beta \leq 1.05$	parallel, $\Theta = 0°$	linear	propagating *shock* & *S-polarized RD*	*S-polarized RD* or *DD*	depends on $\chi_\parallel$ value; strong: $\|L\| \simeq \|\lambda\|$	at $\tau \sim 1$ small-scale, noisy waveforms radiated
		circular	phase irregularities & circ.-polarized wave	circ.-polarized wave		
Gyro-kinetic and Landau damping, $.5 \leq \beta \leq 1.5$	oblique, $\Theta \sim 30°$	linear	*S-polarized* RD's (broad)	*S-* or *lin.*-polarized waves	strong	*cyclotron* wave-part. interaction at high-k
		circular	weakly modulated circular wave	pure circular wave	weak	$\sim\sim\sim\sim\sim\sim\sim$ *inhibit* arc- RD formation

TABLE I. Summary of the numerical solutions.